1-4-2011

Robust Region Tracking in Multi-Agent Systems Utilizing Sliding Mode Control: Theory and Applications

Mark Bacon
MarkBacon@gmail.com

Robust Region Tracking in Multi-Agent Systems Utilizing Sliding Mode Control: Theory and Applications

Mark Edward Bacon

B.S., Rochester Institute of Technology, 2008

A Thesis

Submitted in partial fulfillment of the

Requirements for the Degree of

Masters of Science

at the

University of Connecticut

2010

APPROVAL PAGE

Masters of Science Thesis

Robust Region Tracking in Multi-Agent Systems Utilizing Sliding Mode Control:

Theory and Applications

Presented by

Mark Edward Bacon, B.S.

Major Advisor _____
Nejat Olgac

Associate Advisor _____
Jiong Tang

Associate Advisor _____
Chenyu Cao

Associate Advisor _____
Horea Ilies

University of Connecticut

2010

ACKNOWLEDGEMENTS

I would like to sincerely thank Prof. Nejat Olgac for his continued support and guidance, without whom, this work would not be possible. Additionally, my associate advisors, Prof. Jiong Tang, Prof. Horea Ilies and Prof. Chengyu Cao, deserve thanks for their time and effort in their critique of this work. Many thanks to the members of the ALARM Lab, Rudy Cepeda Gomez, Jhon Diaz, Zhenyu Zhang, Hesam Babahosseini and Hadi Hajieghrary, for their insights, advice, and companionship in the lab. I would also like to thank my family and friends for their ongoing encouragement and support, without which this achievement would not be feasible.

This work was funded in part by ARO W911NF-07-1-0557

and DHS 2008-ST-061-TS0002

TABLE OF CONTENTS

1. INTRODUCTION **1**

2. SYSTEM DYNAMICS AND PROBLEM FORMULATION **6**

2.1 AGENT-TO-AGENT INTERACTIONS **7**

3. REGION HOLDING SLIDING MODE CONTROLLER (RHSMC) **9**

3.1 CIRCULAR RHSMC **9**

REPULSION FORCE UPPERBOUND FOR CIRCULAR REGIONS 13

CASE STUDIES FOR CIRCULAR REGIONS (Case studies 1 and 2) 15

3.2 ELLIPTICAL RHSMC **21**

REPULSION FORCE UPPERBOUND FOR ELLIPTICAL REGIONS 22

CASE STUDIES FOR ELLIPTICAL REGIONS (Case Study 3) 27

3.3 ARC RHSMC **30**

RADIAL CONTROLLER 33

ANGULAR CONTROLLER 35

CASE STUDY FOR ARC REGION (Case Study 4) 37

4. APPLICATIONS IN HERDING **41**

4.1 EVADER DYNAMICS **42**

4.2 EVADER HERDING FORCE **44**

4.3 PADDLE BASED HERDING IN THE 2v1 CASE **46**

Phase 1 – Alignment, $\mathbf{u}_{j,1}$, $\mathbf{z}_{d1,j}$ 52

Phase 2 – Herding, $\mathbf{u}_{j,2}$, $\mathbf{z}_{d2,j}$ 55

Phase 3 - Containment, $\mathbf{u}_{j,3}$, $\mathbf{z}_{d3,j}$ 55

SUMMARY OF CONTROL LOGIC FOR 2v1 56

CASE STUDY 5: 2v1 Ellipse Based Herding 57

4.4 PADDLE BASED HERDING IN THE MvN CASE **61**

CASE STUDY 6: MvN Ellipse Based Herding 64

4.5 DRAWBACKS OF THE PADDLE BASED POSITIONING METHOD **68**

4.6 ARC BASED RHSMC FOR 2v1 HERDING **69**

CASE STUDY 7: 2v1 Arc Based Herding 73

4.7 ARC BASED HERDING IN THE MvN CASE **79**

CASE STUDY 8: MvN Arc Based Herding 82

5. CONCLUSIONS **86**

REFERENCES **89**

LIST OF FIGURES AND TABLES

FIGURE 1: Inter-agent repulsion force profile 8
FIGURE 2: Circular distribution of 30 agents 14
FIGURE 3: Neighborhood of agent A and the resulting repulsion force 15
TABLE 1: Parameters for Case Studies 1-3 16
FIGURE 4: Case Study #1, 30 agents driven to a fixed target circle 17
FIGURE 5: Case Study #2, 60 Agents tracking a moving circular region 19
FIGURE 6: Sliding function of a single agent from Case Study #2 20
FIGURE 7: Forces exerted on a single agent in Case Study #2 20
FIGURE 8: 80 Agents in a worst case distribution within an ellipse 23
FIGURE 9: Area of scheduled control gains 23
FIGURE 10: Well distributed elliptical configuration 24
FIGURE 11: Force variation among agents at the periphery. 25
FIGURE 12: Ratio of force at p_2 *and* p_1 *for varying ellipse geometries* 26
FIGURE 13: 80 Agents tracking a moving elliptical region 28
FIGURE 14: Sliding function of a single agent during Case Study #3 29
FIGURE 15: Control and repulsion forces Case Study #3 30
FIGURE 16: Arc Region Definition 31
FIGURE 17: sat2(s,a,b) function 36
TABLE 2: Parameters for Case Study 4 38
FIGURE 18: 10 Agents tracking a moving arc region 39
FIGURE 19: Sliding functions of all agents in Case Study 4 40
FIGURE 20: $\mathbf{f}_{ep,i,j}$ *repulsive force profile* 43
FIGURE 21: $\mathbf{f}_{ee,i,k}$ *interaction force profile* 43
FIGURE 22: Illustrating the desired pursuer positions 46
FIGURE 23: Loci of pursuer positions for varying magnitudes of $\mathbf{f}^*$ 48
FIGURE 24: Small changes in the herding force lead to rapid rotations 48
FIGURE 25: Transition between control phases 51
FIGURE 26: Phase 1 final desired positions 53
FIGURE 27: Phase 1 time trace for a stationary evader 54
TABLE 3: Parameters for Case Study 5 58

FIGURE 28: Time trace of Case 5 58
FIGURE 29: Control Phase 59
FIGURE 30: Evader Error 60
FIGURE 31: Evader Control Forces 60
TABLE 4: Parameters for Case Study 6 65
FIGURE 32: Snapshots of case study 5 at t = 0, 1, 2, 3, 4, 12 seconds 66
FIGURE 33: Position and Velocity evader error error 67
FIGURE 34: Evader control forces 67
FIGURE 35: Two pursuers placed on the frontal arc 70
TABLE 5: Parameters for Case Study 7 74
FIGURE 36: Simulation snapshots for case study 6 75
FIGURE 37: Desired herding force and executed repulsive forces 76
FIGURE 38: Evader error e_e variation 77
FIGURE 39: Control action on pursuers 78
FIGURE 40: Sliding function variations and the boundary layers 78
FIGURE 41: 7 pursuers surrounding 1 evader 79
TABLE 6: Case study 8 parameters 83
FIGURE 42: 10 Pursuer- 10 evader positions during herding. 84
FIGURE 43: Evader error 84
FIGURE 44: Pursuer sliding functions 85

1. INTRODUCTION

Recently, decentralized control of multiple robotic agents has become an active area of research [1]. This is in no small part due to the advent of Autonomous Ground Vehicles ('AGVs') and Autonomous Unmanned Aerial Vehicles ('UAVs'). These vehicles have several notable advantages which make them particularly useful. Firstly, autonomous vehicles may be capable of operating in environments or spaces that are unfit for humans. This especially includes combat scenarios and high risk missions related to battlefield support (mine sweeping and cargo delivery). Secondly, the decentralized control of these agents allows them to operate under scenarios with limited communication and without central authority. Additionally, the nature of decentralized multi-agent groups means that the addition or removal of an autonomous agent through accident, fault, or destruction does not compromise the group's task. Many of the proposed methods for control of these groups of agents are based on the control of 'swarms'. That is, identical controllers are designed for agents within a swarm which try to achieve common tasks such as aligning their heading or arriving at a common position.

Initially many 'swarming' models originated from biological inspiration [2-4], and the control strategies implemented on 'swarms' of autonomous vehicles has grown to tackle a multitude of problems, such as flocking [5-10], formation flight [11], area coverage [12-15], and even hostile interactions with other swarms [16].

The specific act of "*flocking*", where agents attempt to retain some proximity to their neighbors while aggregating into a stable formation, has received significant attention. In 2003, Gazi and Passino proposed a first order model [5-6], in which agents were driven to stable flocking behavior by biologically inspired momenta structures. These momenta profiles consisted of attraction at long range, and repulsion at short range, with an equilibrium position between the two. In 2007, Yao *et al.* extended this concept to a second order model [11]. Their controller ensures that the agents' velocities conformed to desirable momenta profiles by utilizing the robustizing properties of Sliding Mode Control, recreating dynamics similar to those used by in [5,6].

Additional expansions to second order dynamics and kinematic agents are analyzed by others. Jin and Gao [25] analyzed guaranteed bounds of stability for agents with interaction force profiles after adding Proportional-Derivative feedback controls to individual agents. Olfati-Saber handled flocking for a second order model [7] where each agent's motion is determined by artificial potential energy components. A virtual leader is introduced to prevent fragmentation into smaller groups by creating a common attractive target for all agents. The assumption of universal knowledge of the virtual leader by all the agents is shown to be unnecessary in 2009 by Su *et al.* [8].

Tanner *et al.* [9] demonstrates stability of a swarm with no leader for arbitrarily quickly switching network topologies, provided that the swarm remains connected. Later, Zavlanos and Tanner [10] advance their control to enforce the connectivity of the swarm through a hybrid control. This controller uses local

estimates of the network topologies to prevent the deletion of any link that would split the swarm.

Controlled distribution of agents over a wide area (called "*area coverage control*") is studied by Cortes *et al.* [12-14]. These approaches analyze static convex environments which restrict the motion of member agents. The control of the agents is generated as a gradient descent of artificial potential fields generated by nearby agents and environmental boundaries.

A hybrid of flocking and area coverage, control of agents inside a moving region, is studied in Cheah [15] using artificial potential fields. This controller identifies a region in which the agents should distribute themselves, and they then track this moving region while spreading themselves evenly within the area. The work presented in this thesis attempts to solve a similar problem using a different approach, benefiting from the traditional sliding mode controller (SMC) and introducing a unique interpretation of the boundary layer concept. This controller competes against modeling uncertainties and bounded unknown forcing functions. The SMC robustly draws all agents towards the target region's center. However when the agents are inside the region the control is softened allowing the inter-agent repulsive forces to determine the spacing between agents. The region's perimeter is shown to be upheld successfully by properly selecting the control gains and the strategy for softening the control.

This softening is applied through the concept of a 'boundary layer'. Classically, SMC is robust to a desirably small boundary layer [18]. Our novelty lies in the use of a relatively large boundary layer which directly relates to the

target geometric region. When a steady state occurs, all agents in the swarm will be entrapped within that region [24]. The implementation of the boundary layer is done in such a manner that sliding occurs at the same time in all spatial dimensions, which is a desirable feature. The resulting decentralized control guides the agents to achieve area coverage within the moving target. The approach to the target by the agents is asymptotic, and collisions are avoided. Discussions on stability of the controlled dynamics, as well as the disturbance rejection capabilities are included.

An application of this controller is found in the subject of herding (driving one or many agents to a desired position using repulsion forces created by controlled herding agents). Despite applicability to animal herding, crowd control and tactical combat maneuvers, herding has received very little attention in the controls community until recently. Kachroo [21] proposes two rule based algorithms for one ‘dog’ to herd one ‘sheep’ on a discrete 3x3 grid, and analyzes the algorithm’s effectiveness based on the number of discrete steps which result in success. The approach utilized here is a heuristic series of rules based on the current discrete configuration of agents rather than a feedback control however. Jyh-Ming Lien [22-23] looks at the herding of multiple sheep in continuous space with one or multiple herders respectively, while addressing the path planning and computational complexity issues.

In our implementations of herding, we utilize our Region Holding Sliding Mode Control. In order to perform the herding, we first find the required feedback control force for the agent(s) to be herded which will guide them to and along a

desired trajectory. We initially investigate the 2 ‘pursuer’ (‘herder’), 1 ‘evader’ scenario (2v1) to develop our positioning logic. We take two unique approaches to the development of the positioning logic, both designed to use the controller’s strengths. These concepts are then elevated to the MvN scenario by small expansions to the control logic.

In the first implementation, the two unique positions for the pursuers developed in the 2v1 scenario are taken as the desired centers for two groups of pursuing agents. The pursuers then track an elliptical region (intended to act as a ‘paddle’) surrounding these positions and they apply approximately equivalent force on the evaders as if the pursuer and evader swarms were lumped as individual agents. As will be seen, this method suffers several drawbacks in the decentralization, complexity and robustness of the control logic.

The second implementation also utilizes the region holding controller, but instead places the agents along an arc shaped region (determined in a cylindrical coordinate system). This single region replaces the two elliptical region centers previously used and reduces the complexity of the problem immensely.

As a common notation within the text, we denote vectors and matrices with a boldface font, and scalars with italic font. Additionally, we define a difference unit vector, $\hat{\mathbf{v}}_{\mathbf{a},\mathbf{b}} = \dfrac{\mathbf{a}-\mathbf{b}}{\|\mathbf{a}-\mathbf{b}\|}$ for use throughout.

2. SYSTEM DYNAMICS AND PROBLEM FORMULATION

For the development of the region holding controller, we consider a swarm of M controlled agents. These agents are taken to be point masses in an n-D environment. Each agent's dynamics are governed by the following equation

$$m_j \ddot{\mathbf{z}}_j + b_j \dot{\mathbf{z}}_j = \mathbf{u}_j + \mathbf{f}_j^r(W_j) + \mathbf{f}_j^u \in \Re^n \qquad j = 1,2,...M \tag{1}$$

where $\mathbf{z}_j \in \Re^n$ is the position vector of the j^{th} agent. m_j and b_j are the mass and drag coefficients of that agent. These values are assumed to be uncertain, but have some nominal values, $\overline{m}$ and $\overline{b}$, and bounded uncertainties, Δm and Δb, such that

$$\begin{aligned} m_j &= \overline{m} + \tilde{m}_j, \qquad |\tilde{m}_j| \le \Delta m << \overline{m} \\ b_j &= \overline{b} + \tilde{b}_j, \qquad |\tilde{b}_j| \le \Delta b << \overline{b} \qquad j = 1,2,\cdots,M \end{aligned} \tag{2}$$

$\mathbf{f}_j^r(W_j)$ is an inter-agent repulsion force which is unknown to the controller, except for its conservative upperbound $\left\|\mathbf{f}_j^r\right\| \le f_{\max}^r$. These forces are directly linked to the geometric distribution of the agents at any given moment. A focused effort on the formation of these forces and determination of their upperbound is presented later in the text for circular and elliptical regions. The set W_j contains the indices of *neighbors* of agent *j,* defined by $W_j = \left\{k : \left\|\mathbf{z}_j - \mathbf{x}_k\right\| \le r_W, j \ne k\right\}$, where r_W is the radius of the *neighborhood*. Only those agents that are identified by W_j, influence the dynamics of agent *j*. The $\mathbf{f}_j^u$ term in Equation (1) represents an unknown force (indicated by the superscript '*u*'). It is assumed to be smoothly varying with a known upperbound, $\left\|\mathbf{f}_j^u\right\| \le f_{\max}^u$.

The objective of the control, $\mathbf{u}_j$, is to drive all agents from a set of arbitrary initial conditions to within a non-stationary target region. This region is defined by its center, $\mathbf{z}_d(t) \in \Re^n$, and the maximum allowable deviation (radius) in a given direction. The control should be robust against modeling uncertainties (the mass and the drag constants) as well as the uncertain repulsion and disturbance forces. Initially, we will consider the target region to be a circle, and later the concept will be extended to elliptical and arc-shaped regions.

2.1 AGENT-TO-AGENT INTERACTIONS

The controlled agents in this problem feel repulsive forces due to other agents, which allows them to create 'personal space', as well as avoid collisions by pushing the neighbors away. The resultant of such inter-agent forces on agent *j* is denoted by $\mathbf{f}_j^r$. These forces come from those agents within the neighborhood of *j* and they meet the following criteria; the force is continuous along $\|\mathbf{z}_j - \mathbf{z}_k\| \in (0, r_W]$, attains its maximum at $\|\mathbf{z}_j - \mathbf{z}_k\| = 0$, and diminishes at the edge of the neighborhood: $\mathbf{f}_j^r\Big|_{\|\mathbf{z}_j - \mathbf{z}_k\| = r_W} = 0$. Unlike traditional swarming interaction forces, there is no need for a long-range attractive force in this problem; instead the control force will act to bring the agents together towards a common desired target.

For the initial development of the control, we assume the formation of these forces as quadratic functions which increase in intensity as the agents get closer together

$$\mathbf{f}_j^r = \sum_{k \in W_j} \mu\left(r_W - \left\|\mathbf{z}_j - \mathbf{z}_k\right\|\right)^2 \hat{\mathbf{v}}_{\mathbf{z}_j,\mathbf{z}_k} \tag{3}$$

where μ is an amplification gain. This force profile is shown in Figure 1. These forces are unknown to the agents except the pessimistic aggregate upper bound. As such, in the control logic they are treated as part of the bounded uncertainty.

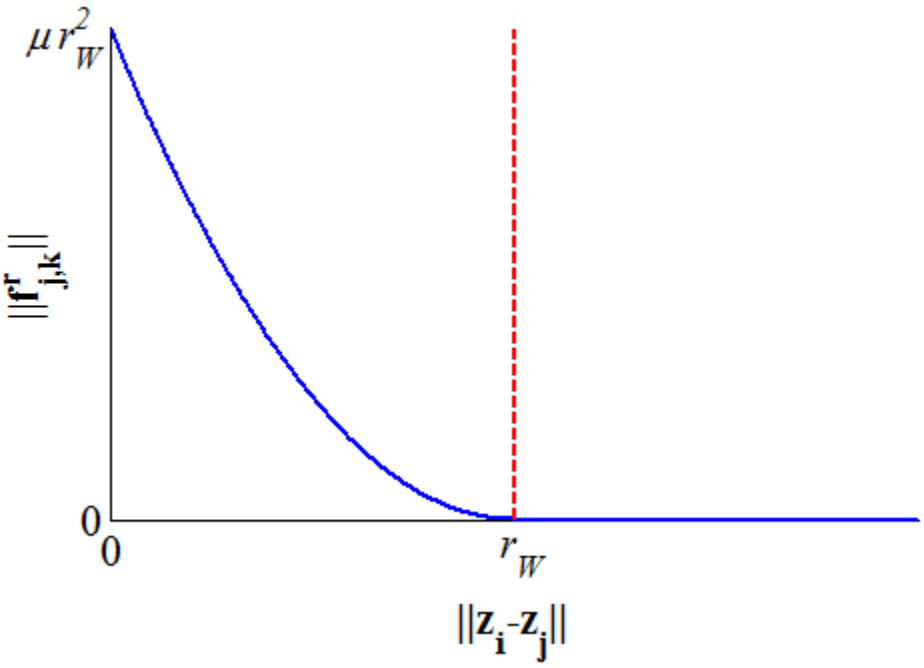

FIGURE 1: Inter-agent repulsion force profile

3. **REGION HOLDING SLIDING MODE CONTROLLER** (RHSMC)

3.1 CIRCULAR RHSMC

The objective of the control is to bring the agents to within the target region, which is taken as a circle. Following traditional SMC formulations [17-19] we start with the definition of error to be minimized,

$$\mathbf{e}_j = \mathbf{z}_j - \mathbf{z}_d \in \Re^n \tag{4}$$

which is the vector connecting an individual agent to the center of the target region, $\mathbf{z}_d(t)$. The sliding function is then defined as a Hurwitz combination of the error.

$$\mathbf{s}_j = \lambda \mathbf{e}_j + \dot{\mathbf{e}}_j \in \Re^n \tag{5}$$

The objective of the sliding mode controller is to reduce $\|\mathbf{s}_j\|$ during the *'approach phase'*, and maintain $\|\mathbf{s}_j\|$ within a confinement in the pursuant '*sliding phase*'. We note that confining $\|\mathbf{s}_j\|$ to a desirably small area will cause first order decay in the error dynamics present in Equation (5). In both phases we utilize LaSalle's theorem [20], to enforce the attractivity to this confinement. A positive definite Lyapunov candidate for agent *j* is proposed as

$$V_j = \tfrac{1}{2}\mathbf{s}_j^T\mathbf{s}_j > 0 \tag{6}$$

In order to ensure the decay of $\|\mathbf{s}_j\|$ we demand that the derivative of this candidate is be negative

$$\dot{V}_j = \mathbf{s}_j^T\dot{\mathbf{s}}_j < 0 \tag{7}$$

Combining Eqs. (1), (4) and (5), results in

$$\dot{\mathbf{s}}_j = \lambda\dot{\mathbf{e}}_j + \tfrac{1}{m_j}\left[\mathbf{u}_j + \mathbf{f}_j^r + \mathbf{f}_j^u - b_j\dot{\mathbf{z}}_j\right] - \ddot{\mathbf{z}}_d \tag{8}$$

The control, $\mathbf{u}_j$, is selected such that the $\mathbf{s}_j$ dynamics in equation (8) behave according to $\dot{\mathbf{s}}_j = -K_1 \cdot \mathbf{s}_j - K_2 \frac{\mathbf{s}_j}{\|\mathbf{s}_j\|}$, which fulfills the condition in (7). To simplify the evaluation of the control, we initially examine the proposed $\mathbf{s}_j$ dynamics in the case of no modeling uncertainty, $\Delta m = 0, \Delta b = 0$. The control is selected to remove any known undesirable terms from (8) and insert the desired dynamics,

$$\mathbf{u}_j = b_j\dot{\mathbf{z}}_j - m_j\left[\lambda\dot{\mathbf{e}}_j - \ddot{\mathbf{z}}_d + K_1\mathbf{s}_j + K_2\frac{\mathbf{s}_j}{\|\mathbf{s}_j\|}\right] \tag{9}$$

Note that the control does not contain $\mathbf{f}_j^r$ or $\mathbf{f}_j^u$ terms as these forces are still taken as unknown. Substituting (9) into (8), we find the following $\mathbf{s}_j$ dynamics

$$\dot{\mathbf{s}}_j = -K_1\mathbf{s}_j + \left[-K_2\frac{\mathbf{s}_j}{\|\mathbf{s}_j\|} - \mathbf{f}_j^r - \mathbf{f}_j^u\right] \tag{10}$$

In order to ensure (7) for all cases, we consider the worst case contributions of the uncertain forces,

$$\dot{\mathbf{s}}_{j,worst\ case} = -K_1\mathbf{s}_j + \left[-K_2 + f_{\max}^r + f_{\max}^u\right]\frac{\mathbf{s}_j}{\|\mathbf{s}_j\|} \tag{11}$$

Selecting $K_2 = f_{max}^r + f_{max}^u$ makes $\dot{\mathbf{s}}_{j,worst\ case} = -K_1\mathbf{s}_j$, which forces $\dot{V}_j < 0$ at all times. A known problem with this method of control is that for small $\|\mathbf{s}_j\|$, the $\frac{\mathbf{s}_j}{\|\mathbf{s}_j\|}$ term in the control (9) brings an undesirable control chatter. This is typically

alleviated with the use of a linear saturation function approximation [17-19] within a small boundary layer $\|\mathbf{s}_j\| \le \varepsilon$.

$$\text{sat}\left(\|\mathbf{s}_j\|, \varepsilon\right) = \begin{cases} 1 & \text{for } \|\mathbf{s}_i\| > \varepsilon \\ \|\mathbf{s}_j\| / \varepsilon & \text{for } \|\mathbf{s}_i\| \le \varepsilon \end{cases} \tag{12}$$

The new control and $\mathbf{s}_j$ dynamics are given as

$$\mathbf{u}_j = b_j \dot{\mathbf{z}}_j - m_j \left[\lambda \dot{\mathbf{e}}_j - \ddot{\mathbf{z}}_d + K_1 \mathbf{s}_j + K_2 \text{sat}\left(\|\mathbf{s}_j\|, \varepsilon\right) \frac{\mathbf{s}_j}{\|\mathbf{s}_j\|} \right] \tag{13}$$

$$\dot{\mathbf{s}}_{j,\,worst\ case} = -K_1 \mathbf{s}_j + \left[-K_2 \text{sat}\left(\|\mathbf{s}_j\|, \varepsilon\right) + f_{\max}^{r} + f_{\max}^{u} \right] \frac{\mathbf{s}_j}{\|\mathbf{s}_j\|} \tag{14}$$

The system is robust outside the boundary layer (where the saturation function evaluates to 1) and the controller (13) is designed to drive the system towards $\|\mathbf{s}_j\| \le \varepsilon$. Investigating (5), we note that after confinement, at a steady state (i.e. $\dot{\mathbf{e}}_j \approx 0$), the error $\mathbf{e}_j$ remains bounded within

$$\|\mathbf{e}_j\| \le \varepsilon / \lambda \tag{15}$$

Our implementation of the boundary layer concept is novel in that ε is finite by definition, as opposed to small in conventional deployment. This provides not only the intended chatter abatement [18-19, 24], but also softens the attraction of the target region's center. Outside this region, the robustizing term is in full effect and drives the agents towards the region. Inside the region however, it is tolerant towards the inter-agent spacing forces (i.e., repulsion).

We now allow for modeling uncertainties and follow an identical analytical path from Equation (9) to Equation (14). The control expression in Equation (13) ecomes

$$\mathbf{u}_j = \bar{b}\dot{\mathbf{z}}_j - \bar{m}\left[\lambda\dot{\mathbf{e}}_j - \ddot{\mathbf{z}}_d + K_1 \cdot \mathbf{s}_j + K_2 \cdot \mathrm{sat}\left(\left\|\mathbf{s}_j\right\|, \varepsilon\right)\frac{\mathbf{s}_j}{\left\|\mathbf{s}_j\right\|}\right] \tag{16}$$

where the known nominal values of m_j and b_j are utilized in place of the exact values. Substituting Equation (16) into Equation (8), the $\mathbf{s}_j$ dynamics and corresponding Lyapunov candidate become

$$\dot{\mathbf{s}}_j = \frac{1}{m_j}\left[\tilde{m}_j\left(\lambda\dot{\mathbf{e}}_j + \ddot{\mathbf{z}}_d\right) + \tilde{b}_j\,\dot{\mathbf{z}}_j - \bar{m}\left(K_1 \cdot \mathbf{s}_j + K_2 \cdot \mathrm{sat}\left(\left\|\mathbf{s}_j\right\|, \varepsilon\right)\frac{\mathbf{s}_j}{\left\|\mathbf{s}_j\right\|}\right) - \mathbf{f}_j^r - \mathbf{f}_j^u\right] \tag{17}$$

$$\dot{V}_j = \tfrac{1}{m_j}\mathbf{s}_j^T\left[\tilde{m}\left(\lambda\dot{\mathbf{e}}_j + \ddot{\mathbf{z}}_d\right) + \tilde{b}\,\dot{\mathbf{x}}_j - \bar{m}\left(K_1 \cdot \mathbf{s}_j + K_2\mathrm{sat}\left(\left\|\mathbf{s}_j\right\|, \varepsilon\right)\frac{\mathbf{s}_j}{\left\|\mathbf{s}_j\right\|}\right) - \mathbf{f}_j^r - \mathbf{f}_j^u\right] \tag{18}$$

To enforce $\dot{V}_j < 0$, at the border of the boundary layer, that is, where $\mathrm{sat}\left(\left\|\mathbf{s}_j\right\|, \varepsilon\right) = 1$, we consider the most pessimistic case for uncertainties and select the robustizing gain as

$$K_2 \geq \tfrac{1}{\bar{m}}\left(f_{\max}^r + f_{\max}^u + \Delta m\left\|\lambda\dot{\mathbf{e}}_j + \ddot{\mathbf{z}}_d\right\| + \Delta b\left\|\dot{\mathbf{z}}_j\right\|\right) \tag{19}$$

This guarantees the attractivity of the swarm to within the target. Since the initial conditions are selected randomly this stabilizing controller is also claimed to reject intermittent disturbances. That is, once these disturbances disappear the

dynamics treat the new initial conditions the same way, and reinforce the regional attraction.

Inside the boundary layer, the $\mathbf{s}_i$ dynamics can be written as

$$\dot{\mathbf{s}}_j + \frac{\bar{m}}{m_j}\left(K_1 + \frac{K_2}{\varepsilon}\right)\mathbf{s}_j = \frac{1}{m_j}\left[-\mathbf{f}_j^r - \mathbf{f}_j^u + \tilde{b}_j\dot{\mathbf{z}}_j + \tilde{m}_j\left[\lambda\left(\dot{\mathbf{z}}_d - \dot{\mathbf{z}}_j\right) + \ddot{\mathbf{z}}_d\right]\right] \equiv \psi \quad (20)$$

Equation (20) represents a low pass filter against ψ, the perturbations made up of the uncertainties. This filter rejects high frequency components of the dynamics emanating from perturbations with a cutoff frequency at

$$\omega_j = \frac{\bar{m}}{m_j}\left(K_1 + \frac{K_2}{\varepsilon}\right) \quad (21)$$

This strategy is effectively utilized in [19] as well, and experimentally validated.

REPULSION FORCE UPPERBOUND FOR CIRCULAR REGIONS

The upper-bound, f_{max}^r, in Equation (19) represents the largest resultant force exerted on an agent due to the inter-agent repulsions and it is assumed known a priori. We present a numerical procedure to assess that value in 2-D space. The evaluation is dependent on the region in question, and we begin with the evaluation of a circle of radius r_{circ}. When the agents are forced within the target circle, they are expected to space out in a nearly uniform manner. Consequently, those agents at the periphery would be exposed to larger net repulsion forces than those inside. To estimate an extremum for these forces, i.e., f_{max}^r, we create a trial distribution of uniformly spaced agents within the circular target region. This formation is created by positioning the agents over nested

circles with roughly uniform spacing (i.e., $\delta_1 \approx \delta_2 \approx \delta_r$ in Fig. 2 for 30 agents.). We then numerically determine the resultant repulsion forces, using Equation (3), on agents at the periphery (e.g., A in Fig. 3) due to agents in the neighborhood (shaded in the figure). Considering isotropic and uniform distribution of agents within a circle, all peripheral agents should be exposed to similar calculated f^r_{max} values.

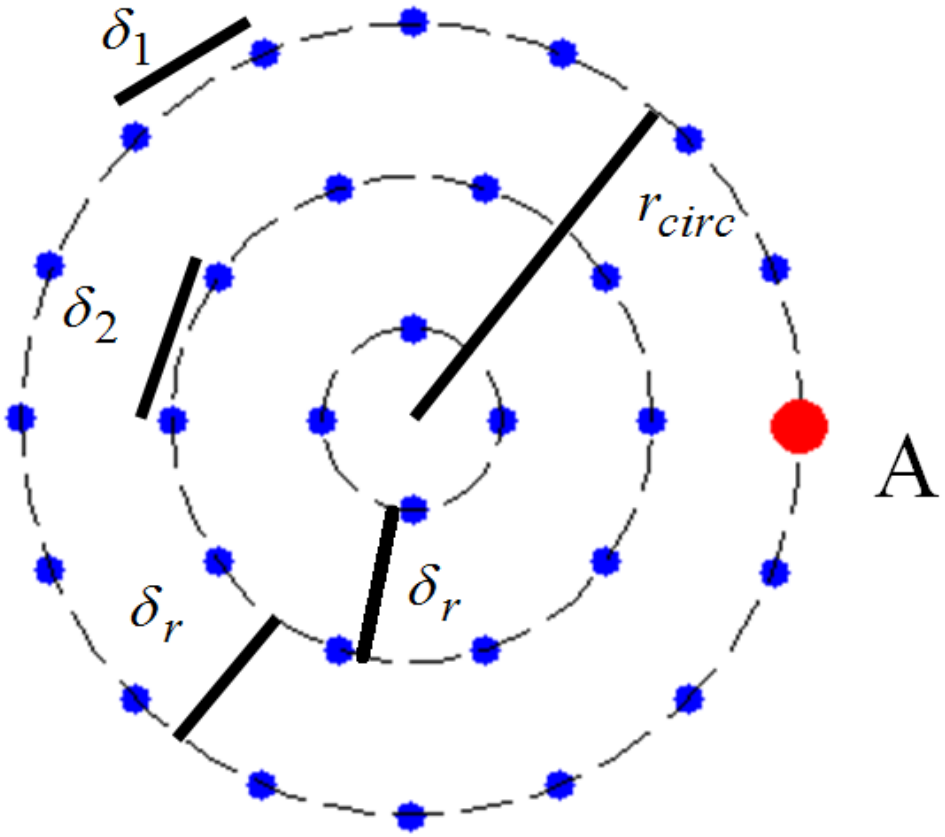

FIGURE 2: Circular distribution of 30 agents

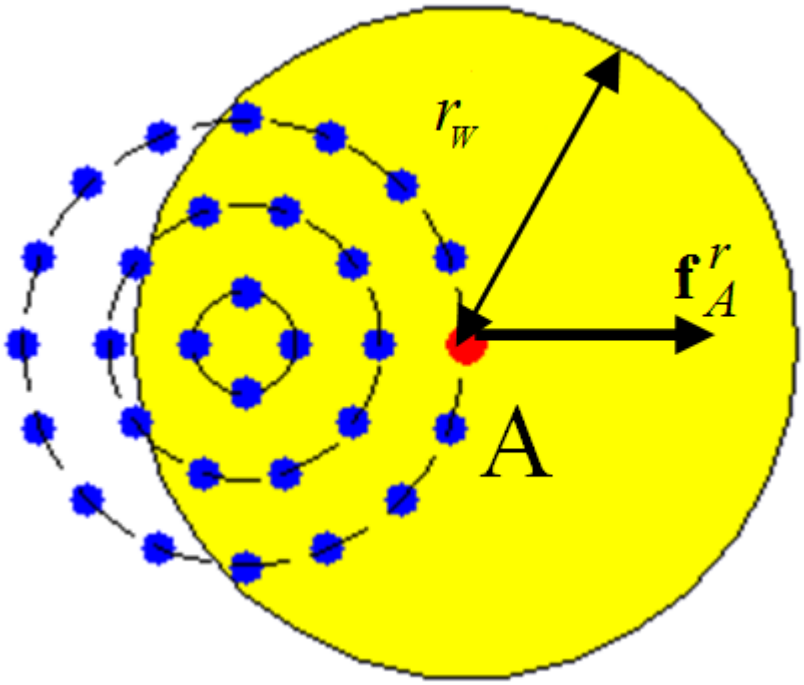

FIGURE 3: Neighborhood of agent A and the resulting repulsion force

CASE STUDIES FOR CIRCULAR REGIONS (Case studies 1 and 2)

In order to demonstrate the effectiveness of the proposed control strategy, we present some case studies. The parameters in table 1 are common to all cases considered. The circular target is again defined by its center, $\mathbf{z}_d(t) \in \Re^2$, and radius, r_{circ}. The boundary layer size, ε, is determined by our required proximity to the center, $\|\mathbf{e}_j\| \le \varepsilon / \lambda = r_{circ}$. Individual m_j and b_j are fixed but randomly selected between different agents based on a uniform probability distribution within the known bounds of uncertainty (Δm and Δb). We also consider an unknown, time-

varying friction-like force, $\mathbf{f}_j^u \equiv -(20+5\sin(2t))\frac{\dot{\mathbf{z}}_j}{\|\dot{\mathbf{z}}_j\|}$ which has a known upperbound $f_{max}^u = 25$.

$\overline{m} = 1$	$\Delta m = 0.05$	$r_W = 3$
$\overline{b} = 1$	$\Delta b = 0.05$	$\mu = 1$
$\lambda = 1$	$K_1 = 5$	

TABLE 1: SIMULATION PARAMETERS

CASE STUDY 1

Here we study a group of 30 agents aggregating within a non-moving circular region with $r_{circ} = 2$, using the aforementioned evaluation of f_{max}^r. Figure 4 shows the time-lapsed frames of the dynamics. The agents distribute themselves throughout the entire region, which indicates that our prediction of supremum of repulsion forces, f_{max}^r, is appropriate. The first two frames do not have as many agents due to their randomly selected remote starting positions.

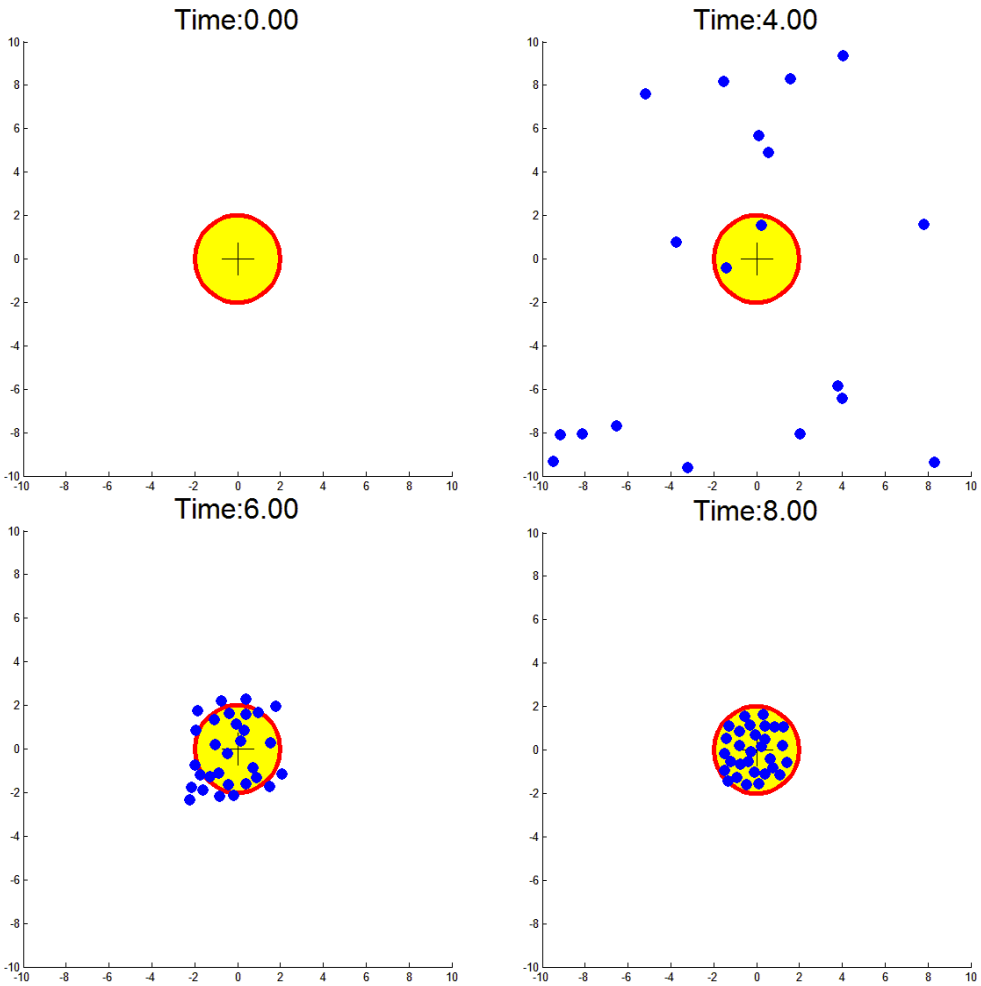

FIGURE 4: Case Study #1, 30 agents driven to a fixed target circle

CASE STUDY 2

(Fig. 5) shows 60 agents tracking a circular region of radius 2, the center of which is moving according to $\mathbf{z}_d = [3\sin(4t) \quad 3\cos(2t)]^T$ which is shown as a trace in Fig. 5. All of the agents again aggregate inside the region despite parameter uncertainties, upper-bounded unknown forces, and inter-agent repulsion forces.

Time traces of $\mathbf{s}_j \in \Re^2$ for a single agent are shown in Fig. 6. The agent enters the *sliding phase* within 0.8 seconds, which roughly corresponds to 4 times

the time constant of $\dot{\mathbf{s}}_{j,worst\ case} = -K_1\mathbf{s}_j$, or $1/K_1 = 0.2$ seconds, starting from large values of $\mathbf{s}_j$. Note the sliding manifold of $\|\mathbf{s}_j\| < 2$ is unnoticeably small in the figure. Figure 7 shows the control force, repulsive forces and the uncertain force on the same agent. We note that at approximately 4 seconds the inter-agent repulsion forces increase. At the same time, the control acts in the opposing direction and at the steady state, the force balance leads the agent to take a constant position with respect to the center of the region. The resultant of *all* forces on the agent at the steady state is periodic in nature, corresponding to the motion of the moving region.

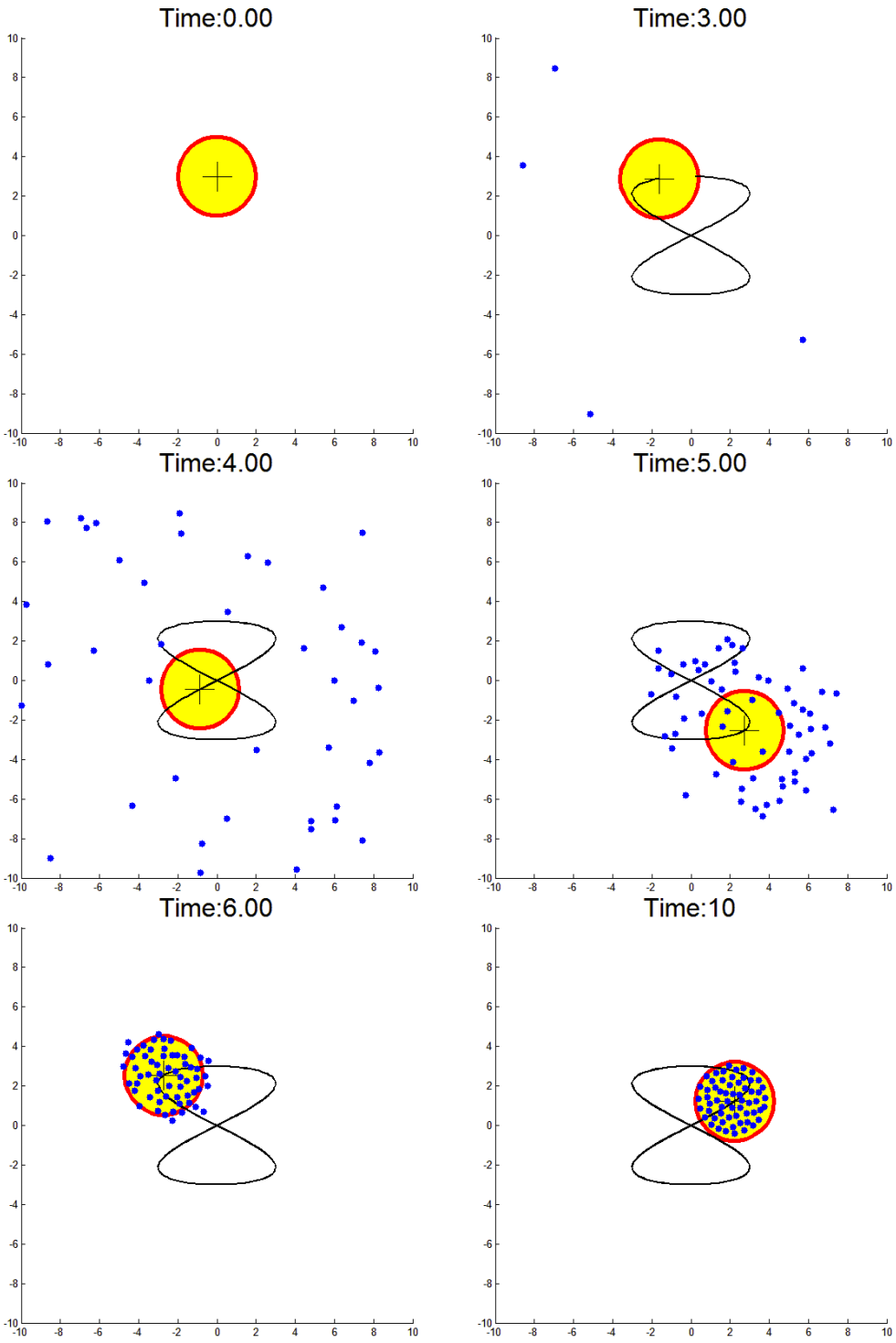

FIGURE 5: Case Study #2, 60 Agents tracking a moving circular region

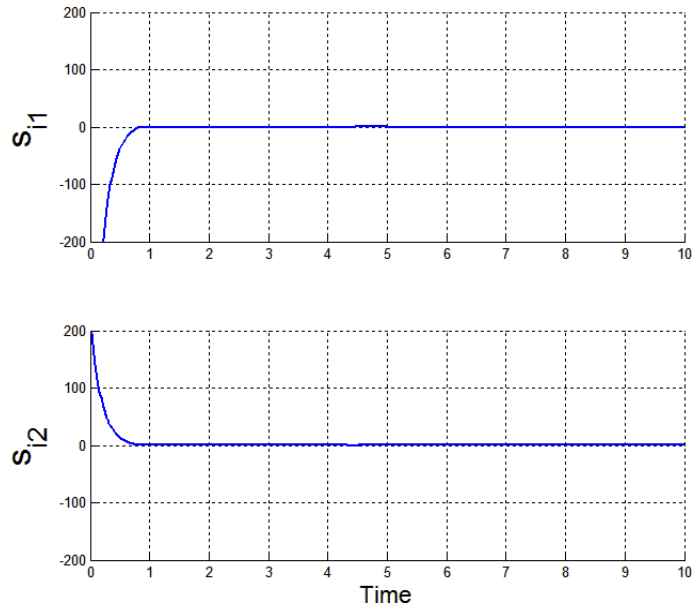

FIGURE 6: Sliding function of a single agent from Case Study #2

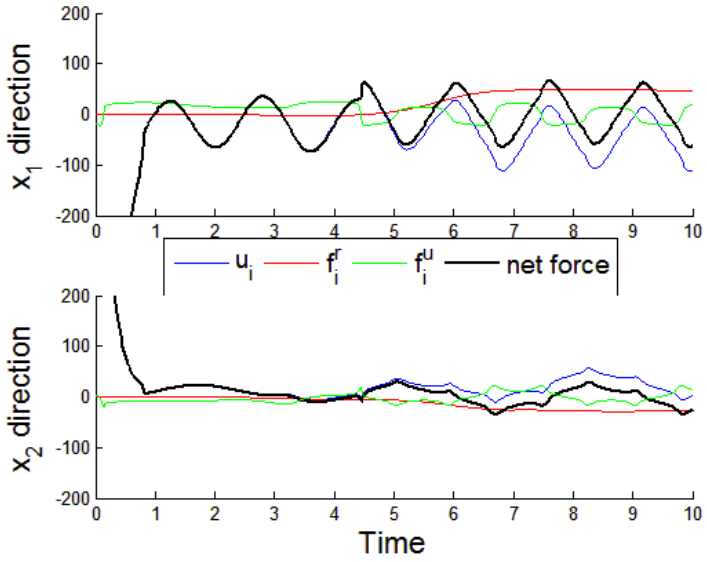

FIGURE 7: Forces exerted on a single agent in Case Study #2

3.2 ELLIPTICAL RHSMC

As a natural extension from the circular distribution previously presented, we expand the analysis to include an elliptical configuration. Again, while we study the operation in 2-D, the concepts can be easily extended for an *n*-D system.

We define the region, by its center $\mathbf{z}_d(t) \in \Re^2$, and the oblique ellipse by $(\mathbf{z}-\mathbf{z}_d)^T \mathbf{T}(\mathbf{z}-\mathbf{z}_d)=1$, where $\mathbf{T} \in \Re^{2x2}$ is a symmetric matrix. This matrix contains information on the scaling factors of major and minor axes (from here on denoted by r_1 and r_2), as well as the angle of the major axis ϕ.

The move to an ellipse requires slight changes to the controller. We again define a boundary layer, but this time as an elliptical region such that it corresponds to the target ellipse. We adopt a new vector norm for this process

$$\|\mathbf{a}\|_T = \sqrt{\mathbf{a}^T \mathbf{T} \mathbf{a}} \tag{22}$$

Next the development of Section 3 is retraced, to deploy the boundary layer concept. The goal is to ensure robust attraction towards the boundary layer (i.e., the target region) $\|\mathbf{s}_j\|_T \le \varepsilon$. That means at the steady state, when the dynamics settle, we expect

$$\|\mathbf{e}_j\|_T \le \varepsilon/\lambda = 1 \tag{23}$$

which implies an entrapment within the elliptical target. In order to achieve this we use the same robust control logic as in equation (16), except utilizing the new norm in the saturation function,

$$\text{sat}\left(\left\|\mathbf{s}_j\right\|_T, \varepsilon\right) = \begin{cases} 1 & \text{for } \left\|\mathbf{s}_j\right\|_T > \varepsilon \\ \left\|\mathbf{s}_j\right\|_T / \varepsilon & \text{for } \left\|\mathbf{s}_j\right\|_T \le \varepsilon \end{cases} \tag{24}$$

Notice that in (16) the robustizing force with K_2 is still acting in the same sense as before, i.e., assisting $\mathbf{s}_j^T \dot{\mathbf{s}}_j < 0$.

REPULSION FORCE UPPERBOUND FOR ELLIPTICAL REGIONS

The f_{max}^r quantity is again needed as a priori knowledge in the control. A conservative upperbound for this quantity can be obtained if we consider bunching of the agents within a circle of radius r_2 (Fig. 8), instead of evenly distributing them inside the target ellipse. This worst case configuration obviously produces the highest expected density of agent within an ellipse. Because they are being squeezed more forcefully from the minor axis, we expect at least some eccentricity in the formation along the same axis as the ellipse. We evaluate the repulsive forces in this circular configuration using similar arguments as in Fig. 2 and 3.

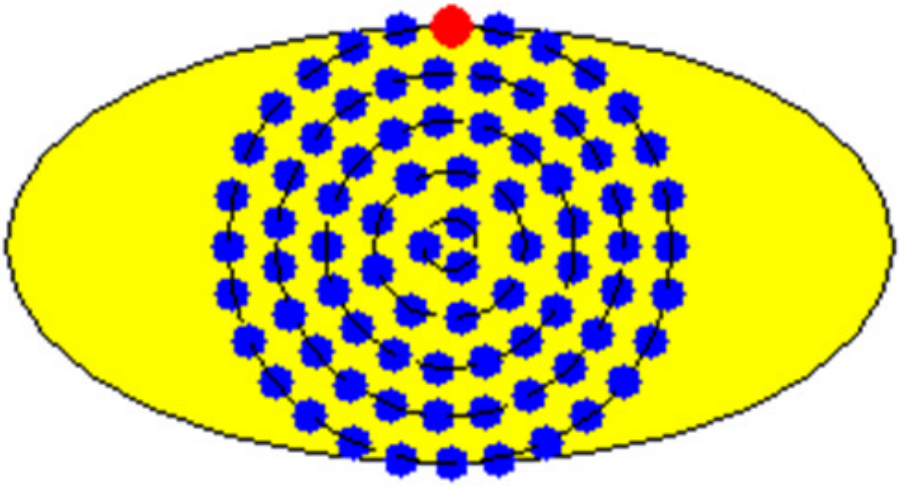

FIGURE 8: 80 Agents in a worst case distribution within an ellipse

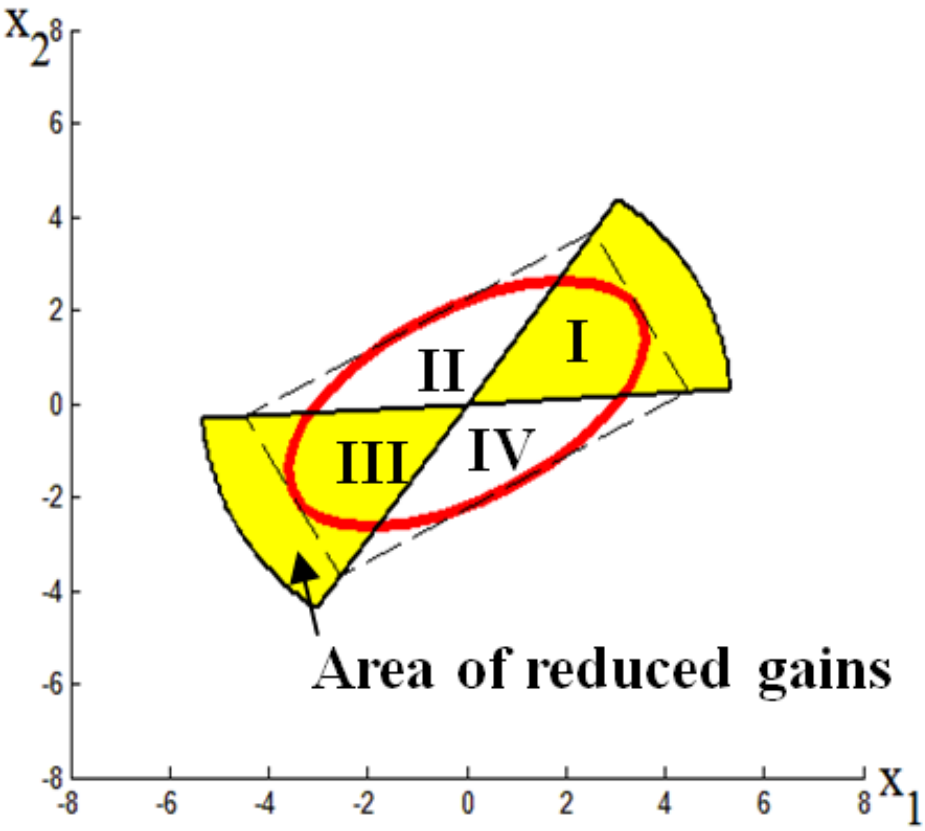

FIGURE 9: Area of scheduled control gains

In an elliptical distribution, the directional isotropy of the maximum of the repulsive forces is lost. Therefore we divide the approach phase into 4 separate zones (Fig. 9).

These areas are determined by the aspect ratio of the target ellipse, and are used to schedule the gains, compensating for the lack of isotropy. In order to determine the appropriate gain reduction, we create a trial distribution which fully fills the ellipse (shown in Figure 10). Figure 11 shows how the repulsive forces vary when agents are distributed evenly within the entire elliptical region (with $r_1 = 4$ and $r_2 = 2$). Note that the slight asymmetry present in this figure is due to the selected distribution of the agents which is not perfectly symmetric. However, the maximum repulsive forces in regions I and III are very close (as well as those in II and IV), and they are taken as equal.

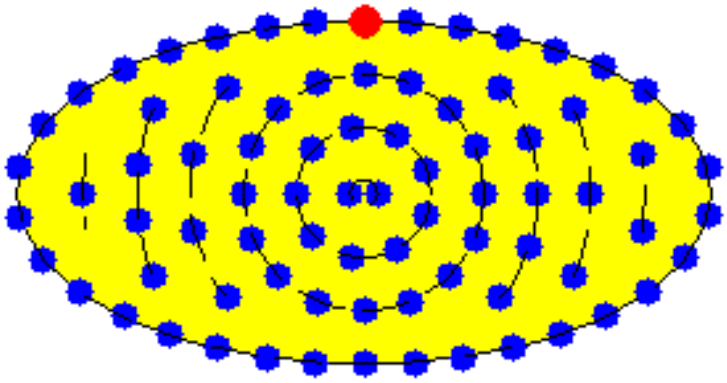

FIGURE 10: Well distributed elliptical configuration

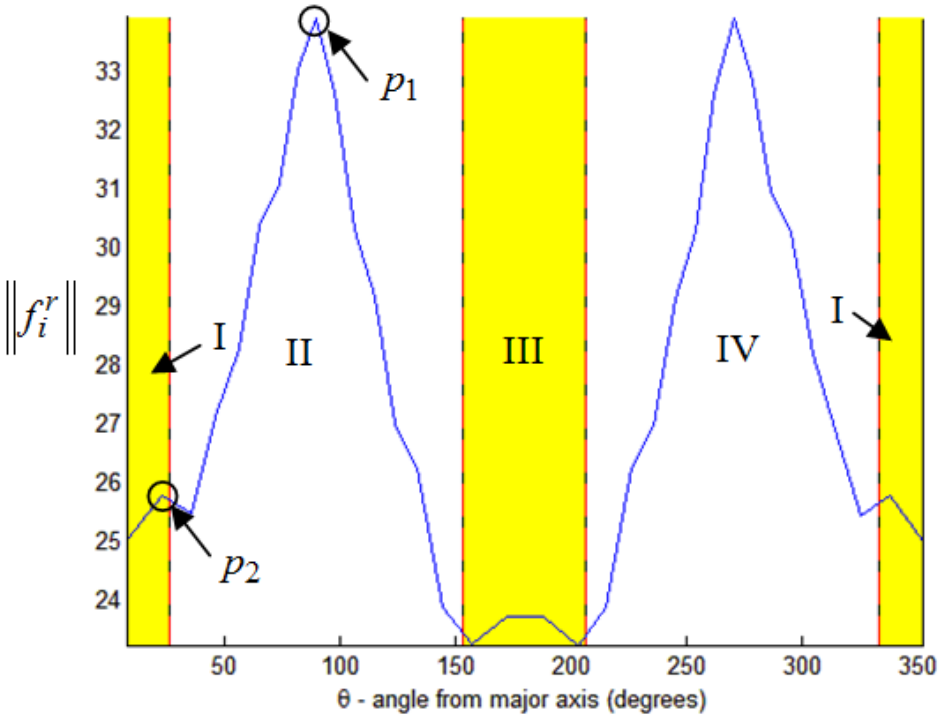

FIGURE 11: Force variation among agents at the periphery of the elliptical distribution in Figure 10.

To accommodate the difference in repulsive forces in different regions, we utilize the worst-case scenario (determined using Fig. 8) in zones II and IV, and scale the outcome down for zones I and III according to the ratio of the forces at p_1 and p_2.

The precise value of this ratio for a given ellipse and radius of interaction is unnecessary however, as a simple approximation can be substituted. Figure 12 shows the ratio of the force at p_2 to the force at p_1 for configurations with varying interaction radii and major and minor axes, with eccentricities between 0 and 0.94. This figure was created by generating sample elliptical configurations and

evaluating the maximum of repulsive forces in the different regions. This was performed for 100, 200, 300, 400 and 500 agents, and the plot below illustrates the average of these distributions, reducing the dependence on *M*. Eccentricities higher than 0.94 were not considered due to numerical and coding complexities arising in these thin ellipses.

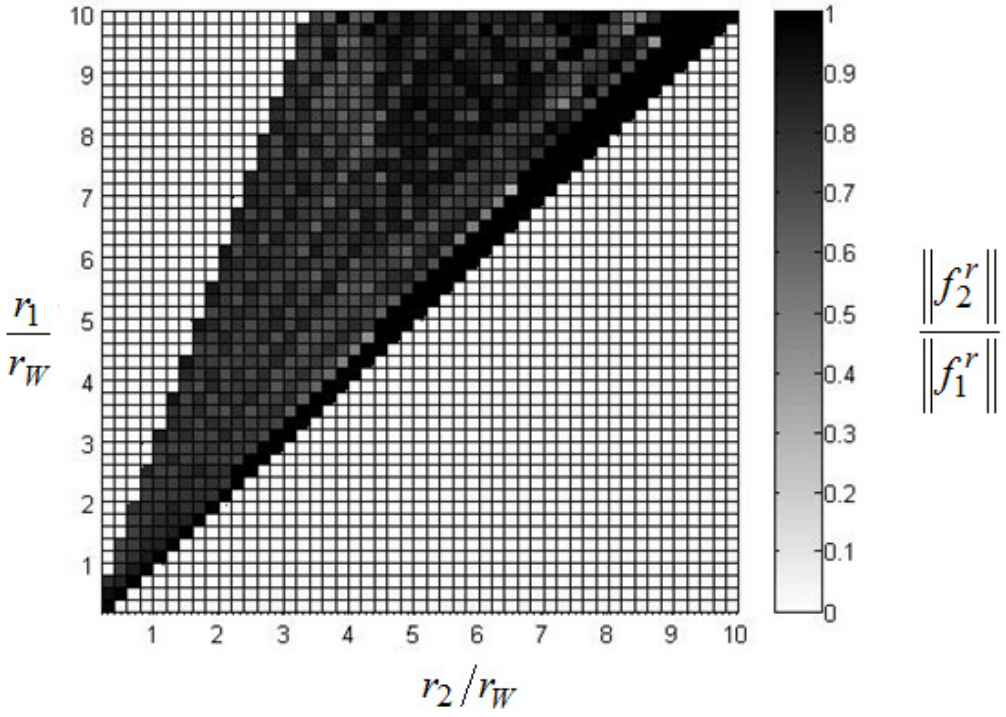

FIGURE 12: Ratio of force at p_2 and p_1 for varying ellipse geometries

The figure shows a relatively flat ratio, which averages to 0.83 for eccentricities between 0.40 and 0.94 (the majority of the shaded region), and this ratio is recommended for use. Bear in mind that we are reducing an already overly-conservative value from Fig. 8, and so the exact ratio for a specific geometry is not necessary to determine a conservative value.

Note also that both $K_1\mathbf{s}_i$ and $K_2 \cdot \text{sat}\left(\left\|\mathbf{s}_j\right\|_T, \varepsilon\right)\frac{\mathbf{s}_j}{\left\|\mathbf{s}_j\right\|}$ terms in (16) are forces pointing the center of the target ellipse. Because of the sizable boundary layer, the $K_1\mathbf{s}_j$ term is non-negligible at the border of the region. In order to create the elliptical distribution, the K_1 term is also scheduled in the four regions (I-IV) based on the proportionality of the f_{max}^r selections for the respective regions as described above.

CASE STUDIES FOR ELLIPTICAL REGIONS (Case Study 3)

We see the results of an elliptical case study illustrated in Fig. 13, using an elliptical region with major axis $r_1 = 4$, minor axis $r_2 = 2$, and obliqueness $\phi = \pi/6$. The matrix $\mathbf{T} = \begin{bmatrix} .1094 & -.0812 \\ -.0812 & 0.2031 \end{bmatrix}$ contains this information, and the target region again follows a similar desired trajectory (shown by a trace) $\mathbf{z}_d = [3\sin(4t) \quad 3\cos(2t)]^T$. We use 80 agents, and again add a force $\mathbf{f}_j^u = -(20 + 5\sin(2t))\frac{\dot{\mathbf{z}}_j}{\left\|\dot{\mathbf{z}}_j\right\|}$ of which only the upper bound $f_{max}^u = 25$ is known to the controller. Remaining parameters are pulled from Table 1.

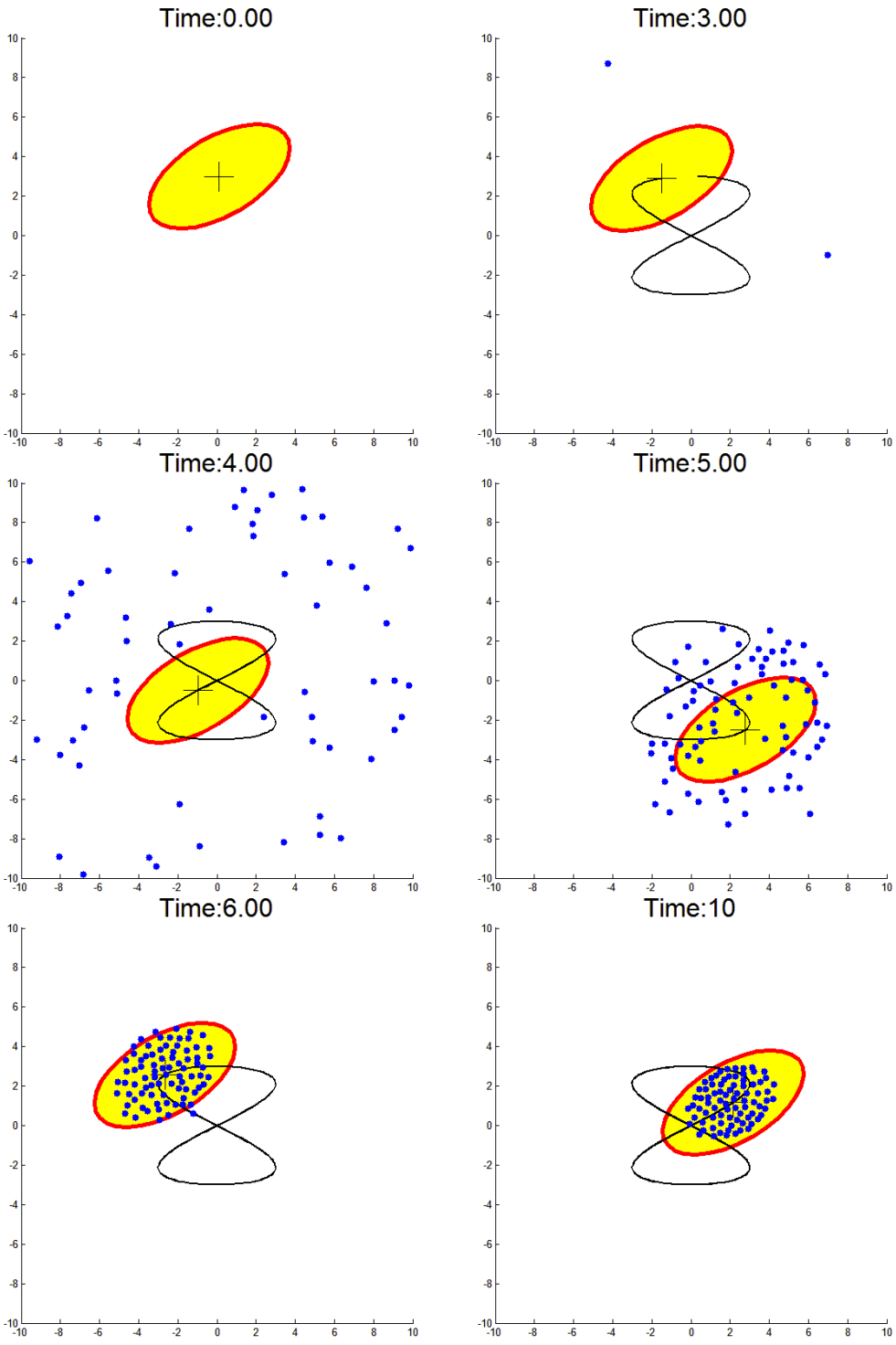

FIGURE 13: 80 Agents tracking a moving elliptical region

After 10 seconds, all the agents are collected inside the region. The area near the end of the major axis is not fully occupied, and agents are somewhat bunched near the middle due to the formation of estimated f_{max}^{r} which is more over-conservative along the major axis (regions I and III in Fig. 9) than it is in the transverse direction (regions II and IV). Nevertheless, the agents are attracted to within the desired target region together with their neighbors.

Figures 14 and 15 show the time variations of the sliding function and the control forces respectively. We notice similar dynamics to those in case study 2: the sliding occurs after approximately 0.8 seconds. The net force at the steady state is again periodic in nature, related to that of region's motion.

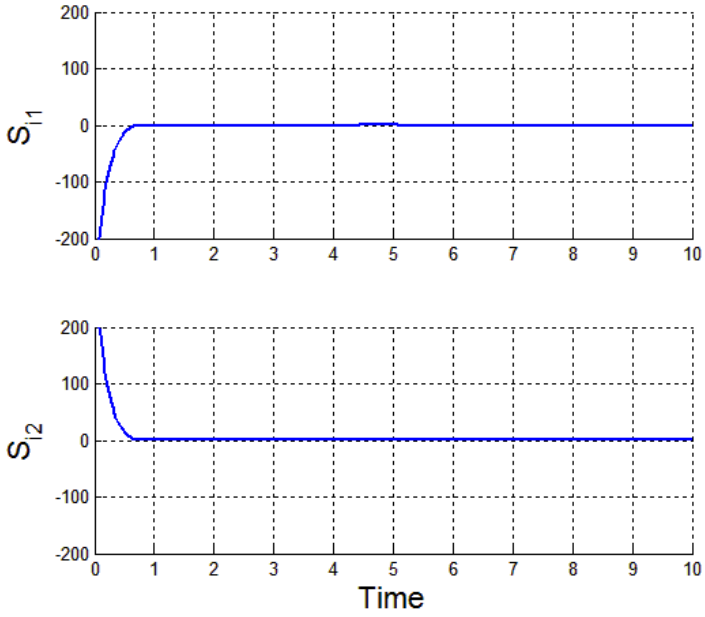

FIGURE 14: Sliding function of a single agent during Case Study #3

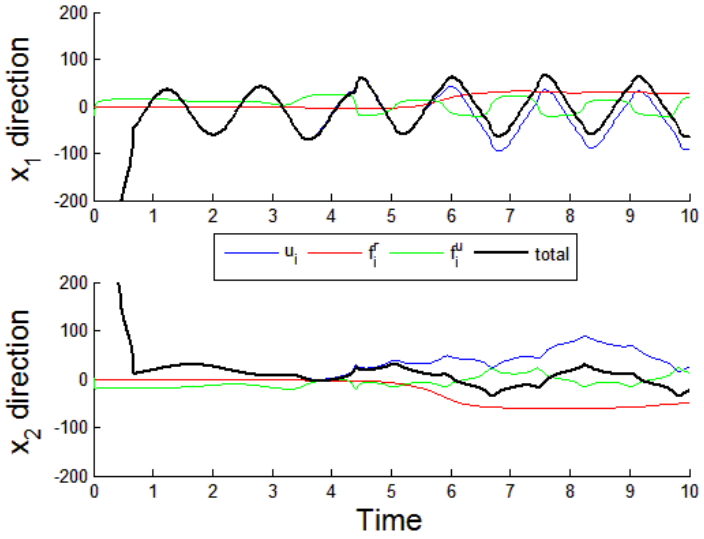

FIGURE 15: Control and repulsion forces on a single agent during Case Study #3

These results were presented at the 2010 ASME Dynamic Systems and Controls Conference in Boston MA, [24].

3.3 ARC RHSMC

Finally, we extend the concepts of the Region Holding SMC to an arc shape. This extension illustrates the ability of the controller to form non-convex regions through the use of different coordinate systems.

We define the agent dynamics relative to a moving arc center, $\mathbf{y}$, as follows

$$\mathbf{z}_j - \mathbf{y} = r_j(t)\,\hat{\mathbf{v}}_{\mathbf{z}_j,\mathbf{y}} \qquad j = 1,2 \tag{25}$$

where, $r_j = \|\mathbf{z}_j - \mathbf{y}\|$. $\hat{\mathbf{v}}_{\mathbf{z}_j,\mathbf{y}} = \hat{\mathbf{e}}_r = [\cos(\theta_j) \;\; \sin(\theta_j)]^T$ is the directional unit vector of $\mathbf{z}_j - \mathbf{y}$. In order to define an arc shaped region, we define a desired radius with a

tolerance, $r_d \pm \Delta r$, and a desired angle with a tolerance, $\theta_d \pm \Delta\theta$, both shown in figure 16.

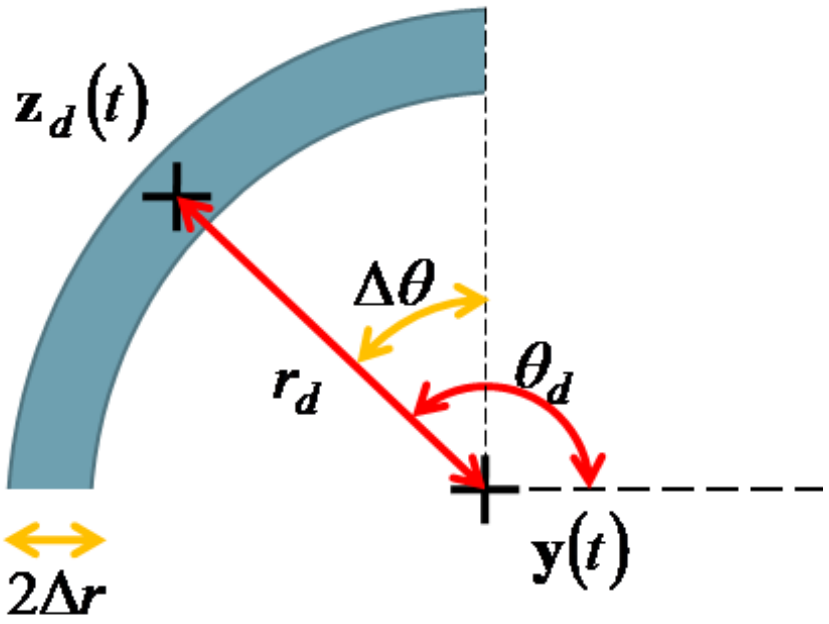

FIGURE 16: Arc Region Definition

Taking the 2nd time derivative of equation (25) one obtains

$$\ddot{\mathbf{z}}_j - \ddot{\mathbf{y}} = \left(\ddot{r}_j - r_j\dot{\theta}_j^2\right)\hat{\mathbf{e}}_r + \left(2\dot{r}_j\dot{\theta}_j + r_j\ddot{\theta}_j\right)\hat{\mathbf{e}}_\theta \qquad j = 1,2 \qquad (26)$$

Combining (1) and (26) :

$$\frac{1}{m_p}\left[\mathbf{u}_j + \mathbf{f}_{pp,j,k\neq j} - b_p\dot{\mathbf{z}}_j\right] - \ddot{\mathbf{y}} = \left(\ddot{r}_j - r_j\dot{\theta}_j^2\right)\hat{\mathbf{e}}_r + \left(2\dot{r}_j\dot{\theta}_j + r_j\ddot{\theta}_j\right)\hat{\mathbf{e}}_\theta \qquad (27)$$

The control is proposed as follows,

$$\mathbf{u}_j = b_p\dot{\mathbf{z}}_j + m_p\left[\ddot{\mathbf{y}} - r_j\dot{\theta}_j^2\hat{\mathbf{e}}_r + u_{j,r}\hat{\mathbf{e}}_r + 2\dot{r}_j\dot{\theta}_j\hat{\mathbf{e}}_\theta + u_{j,\theta}\hat{\mathbf{e}}_\theta\right] \qquad (28)$$

which reflects all of the measurable components in the dynamics (27), as well as two currently undefined control components, $u_{j,r}$ and $u_{j,\theta}$, for the robustizing Sliding Mode Controller in the radial and angular directions, respectively. The substitution of equation (28) into equation (27) results in

$$\tfrac{1}{m_p}\mathbf{f}_{pp,j,k\neq j} + u_{j,r}\hat{\mathbf{e}}_r + u_{j,\theta}\hat{\mathbf{e}}_\theta = \ddot{r}_j\hat{\mathbf{e}}_r + r_j\ddot{\theta}_j\hat{\mathbf{e}}_\theta \qquad j,k = 1,2 \qquad (29)$$

Equation (29) can be rewritten in radial and angular components as

$$\ddot{r}_j = u_{j,r} + \tfrac{1}{m_p}\mathbf{f}_{pp,j,k\neq j} \bullet \hat{\mathbf{e}}_r \qquad (30)$$

$$r_j\ddot{\theta}_j = u_{j,\theta} + \tfrac{1}{m_p}\mathbf{f}_{pp,j,k\neq j} \bullet \hat{\mathbf{e}}_\theta \qquad (31)$$

The repulsive forcing terms in (30, 31) are specific to the particular distribution of the agents, and therefore it is unknown to the pursuer *j*. They do have an upperbound however, as we discuss below. These forces are treated as uncertainties in formulating robust and decentralized control logic for the j^{th} pursuer.

We define next the agent positioning error in the radial and angular directions as

$$e_{j,r} = r_j - r_d \qquad (32)$$

$$e_{j,\theta} = \theta_j - \theta_d \qquad (33)$$

In the radial direction, we wish to minimize this error, thereby placing all agents on the arc. In the angular direction however, we only wish to ensure that the error is bounded within $\pm\Delta\theta$ restricting the pursuers to lie inside the angular extremes of the frontal arc.

For the robust control law we follow the classical Sliding Mode Control (SMC) procedures given in [17-19] and [24]. We start with the selections of the sliding function for each coordinate as some Hurwitz combinations of the respective errors,

$$s_{j,r} = \lambda e_{j,r} + \dot{e}_{j,r} \tag{34}$$

$$s_{j,\theta} = \lambda e_{j,\theta} + \dot{e}_{j,\theta} \tag{35}$$

where $\lambda \in \Re^+$ controls the rate of decay in error after the sliding starts. The two positive definite Lyapunov functions corresponding to the two orthogonal directions are chosen as

$$V_{j,r} = \tfrac{1}{2} s_{j,r}^2 \tag{36}$$

$$V_{j,\theta} = \tfrac{1}{2} s_{j,\theta}^2 \tag{37}$$

We wish to design the control in the following segments, such that both of these Lyapunov candidates show negative definite time derivatives.

RADIAL CONTROLLER

The derivative of the first Lyapunov function is

$$\dot{V}_{j,r} = s_{j,r} \cdot \left[\lambda \dot{e}_{j,r} + \ddot{r}_j - \ddot{r}_d \right] \tag{38}$$

which needs to be negative. To ensure this we force the second factor in (38) to behave like

$$\lambda \dot{e}_{j,r} + \ddot{r}_j - \ddot{r}_d = -K_1 s_{j,r} - K_2 \cdot \mathrm{sat1}\left(s_{j,r}, \varepsilon\right) \tag{39}$$

following the steps in [18, 19], with $K_1, K_2 > 0$, the saturation function $\text{sat1}(s,\varepsilon) = \begin{cases} \text{sgn}(s) & for \quad |s| \geq \varepsilon \\ s/\varepsilon & for \quad |s| < \varepsilon \end{cases}$ and the boundary layer, $|s_{j,r}| < \varepsilon$. The resulting radial component of the control becomes

$$u_{j,r} = \ddot{r}_d - \lambda \dot{e}_{j,r} - K_1 s_{j,r} - K_2 \cdot \text{sat1}(s_{j,r}, \varepsilon) \tag{40}$$

In order to guarantee this negativity feature against uncertainties, we consider the most conservative scenario for the unknown forcing term in (30), $f_{pp,\max} = r_p \mu \geq \left\| \mathbf{f}_{pp,j,k \neq j} \right\|$. Eqs. (30) and (38) with this conservative bound, yield the worst possible derivative of the Lyapunov function as

$$\dot{V}_{j,r}\Big|_{worstcase} = s_{j,r} \cdot \left[-K_1 s_{j,r} - K_2 \cdot \text{sat1}(s_{j,r}, \varepsilon) + \tfrac{1}{m_p} f_{pp,\max} \tfrac{s_{j,r}}{|s_{j,r}|} \right] \tag{41}$$

which must remain negative. When $s_{j,r}$ is large, during the approach phase, the $-K_1 s_{j,r}$ term is dominant, and $K_1 > 0$ controls the rate of decay. As $s_{j,r}$ becomes smaller, the approach term is diminished and the selection of $K_2 \geq f_{pp,max}/m_p$ ensures the negativity of equation (41) outside the boundary layer of width ε. These selections enforce the entrapment of the sliding function within the boundary layer, $|s_{j,r}| < \varepsilon$, once it penetrates into this region. If a steady state is reached during this entrapment, i.e., $(\dot{e}_{j,r} \approx 0)$, equation (34) indicates entrapment of the agent's radial error within $\lambda\varepsilon$. It is worth noting that inside the boundary layer, the $s_{j,r}$ dynamics are

$$\dot{s}_{j,r} + \left(K_1 + K_2/\varepsilon\right) s_{j,r} = \tfrac{1}{m_p} \mathbf{f}_{pp,j,k \neq j} \bullet \hat{\mathbf{e}}_r \tag{42}$$

which represents a low pass filter against the uncertain repulsion force, with a cut-off frequency

$$\omega_r = K_1 + {}^{K_2}\!/_{\varepsilon} \tag{43}$$

which can be tailored as desired by the selection of the parameters K_1 and ε. This selection enables the control to attenuate considerably the disturbances at higher frequencies than this cut-off value.

ANGULAR CONTROLLER

The time derivative of the angular Lyapunov candidate function (37) is

$$\dot{V}_{j,\theta} = s_{j,\theta} \cdot \left[\lambda \dot{e}_{j,\theta} + \ddot{\theta}_j - \ddot{\theta}_d\right] \tag{44}$$

Again to assure negativity of this function we propose that the second factor in (44) behave like

$$\lambda \dot{e}_{j,\theta} + \ddot{\theta}_j - \ddot{\theta}_d = -K_3 \cdot \mathrm{sat2}\left(s_{j,\theta}, a, b\right) \tag{45}$$

This proposition combined with (31) results in the evaluation of the robustizing angular control, following similar logic to the radial controller,

$$u_{j,\theta} = r_j \cdot \left[\ddot{\theta}_d - \lambda \dot{e}_{j,\theta} - K_3 \mathrm{sat2}\left(s_{j,\theta}, a, b\right)\right] \tag{46}$$

but this time without an approach term (-*Ks*) and using a different saturation function, sat2 which contains a large deadzone as seen in Fig. 33.

$$\mathrm{sat2}(s,a,b) = \begin{cases} \mathrm{sgn}(s) & for \quad a < |s| \\ [s - (a-b)\mathrm{sgn}(s)]/b & for \quad a - b < |s| \le a \\ 0 & for \quad |s| \le a - b \end{cases} \tag{47}$$

where $a = \lambda \Delta\theta$ and b is a desirably small number $b/a < 1$. The reason for this selection is to prevent the escape from the boundary layer $|s_{j,\theta}| \le a$ while gradually

allowing the repulsion forces to control the pursuer positioning in the entrapment after a small transition zone of *b*. This robustizing force collects the agents within the frontal arc of $2\Delta\theta$ but leaves the distribution within the arc to the inter-agent repulsion forces f_{pp}. This selection incorporates our desired arc length ($2\Delta\theta$) into the decentralized controller.

By trapping the sliding function within this boundary layer, should a near steady state occur $(\dot{e}_{j,\theta} \approx 0)$, we can see from equation (35) that the $|s_{j,\theta}| \le a = \lambda\Delta\theta$ implies the agents are driven (in the angular coordinate) within the arc of $2\Delta\theta$. Once in this bound they are left under the guidance of the inter-agent repulsion forces. At the steady state, they come to rest somewhere on the opposite slopes of $1/b$.

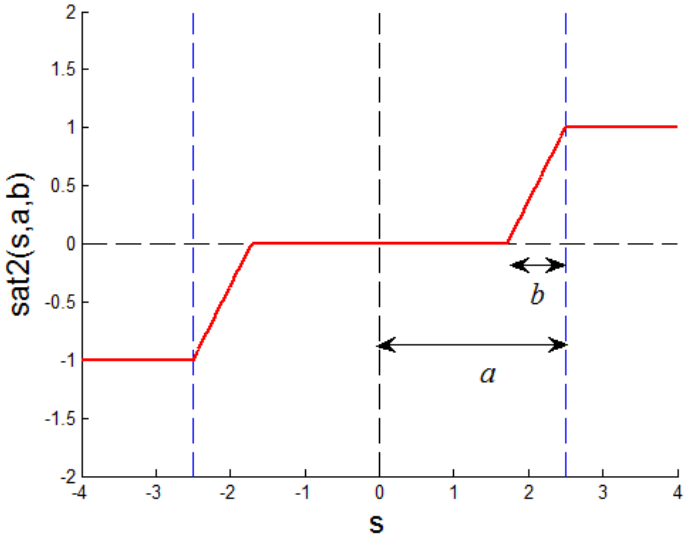

FIGURE 17: sat2(s,a,b) function

Under the combination of radial and angular control laws, each agent is robustly driven within the boundary layer structured by $\left|s_{j,r}\right| < \varepsilon$ and $\left|s_{j,\theta}\right| \le a$, which in turn, characterizes the arc shown in Fig. 16.

The worst case scenario for positive $\dot{v}_{j,\theta}$ should be prevented. For this analysis we combine (31), (44) and (46)

$$\dot{V}_{j,\theta}\Big|_{worst\ case} = s_{j,\theta} \cdot \left[-K_3 \mathrm{sat2}\left(s_{j,\theta}, a, b\right) + \frac{1}{r_j \cdot m_p} f_{pp,\max}\ sign\left(s_{j,\theta}\right) \right] \qquad (48)$$

Clearly the selection of $K_3(t) = f_{pp,\max} / \left[m_p r_j(t)\right]$ suffices for the objective.

We wish to revisit the lack of an approach term, *-Ks,* in the angular controller, unlike the radial controller. Here, we simply guide the agents to remain within the boundary layer of $2\Delta\theta$.without an additional force to bunch them at the center of the arc. The inter-agent repulsive forces take over, as explained above, to evenly spread them to the boundary. Additionally, an approach term is superfluous in this situation as there cannot be an angular error greater than π, which is of the same order of magnitude as the boundary layer.

CASE STUDY FOR ARC REGION (Case Study 4)

In order to demonstrate the effectiveness of the proposed method, we select 10 agents with parameters listed in Table 2 to track an arc with stationary center $\mathbf{y} = [0,0]^T$, desired midpoint, $\theta_d = t$, and desired radius $r_d = 5 + 2\sin(5t)$, and tolerances, $\Delta\theta = \pm\left(\frac{\pi}{4} + \frac{\pi}{8}\sin(5t)\right)$ and $\Delta r = \pm 1$.

$\overline{m}=1$	$\Delta m=0$	$\overline{b}=1$	$\Delta b=0$	$r_W=3$
$\lambda=10$	$K_1=10$	$\mu=20$		

TABLE 2: Parameters for Case Study 4

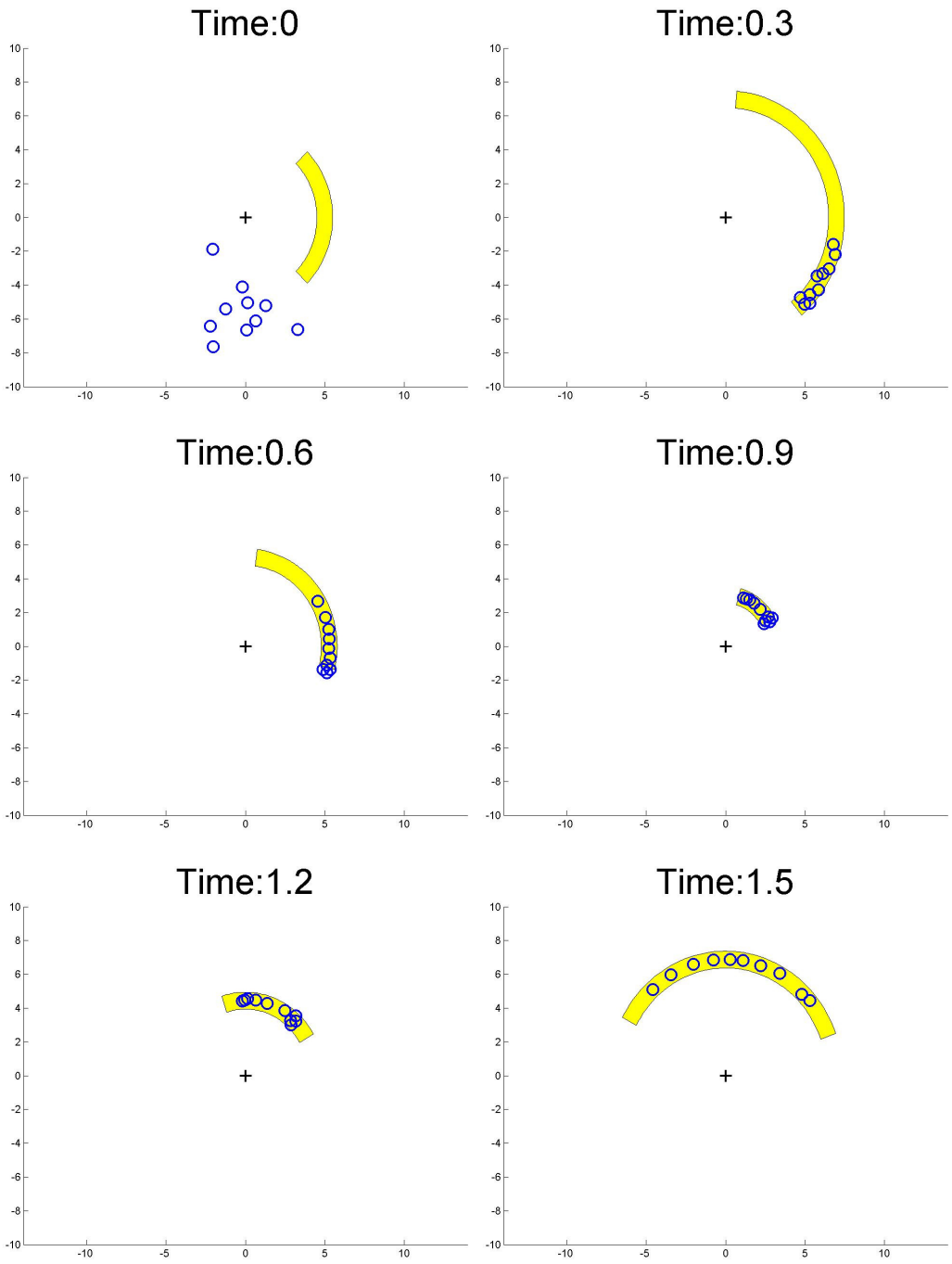

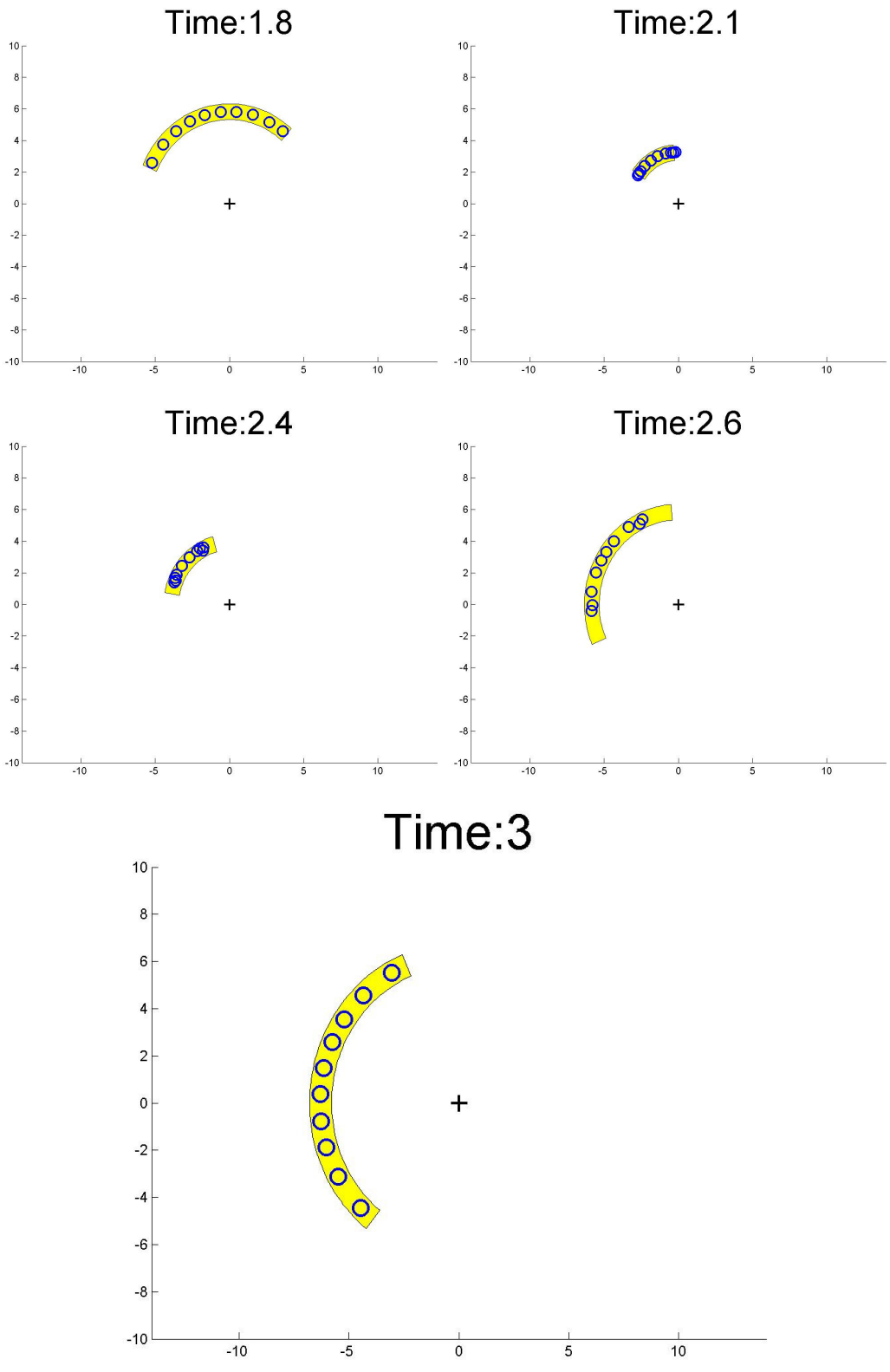

FIGURE 18: 10 Agents tracking a moving arc region

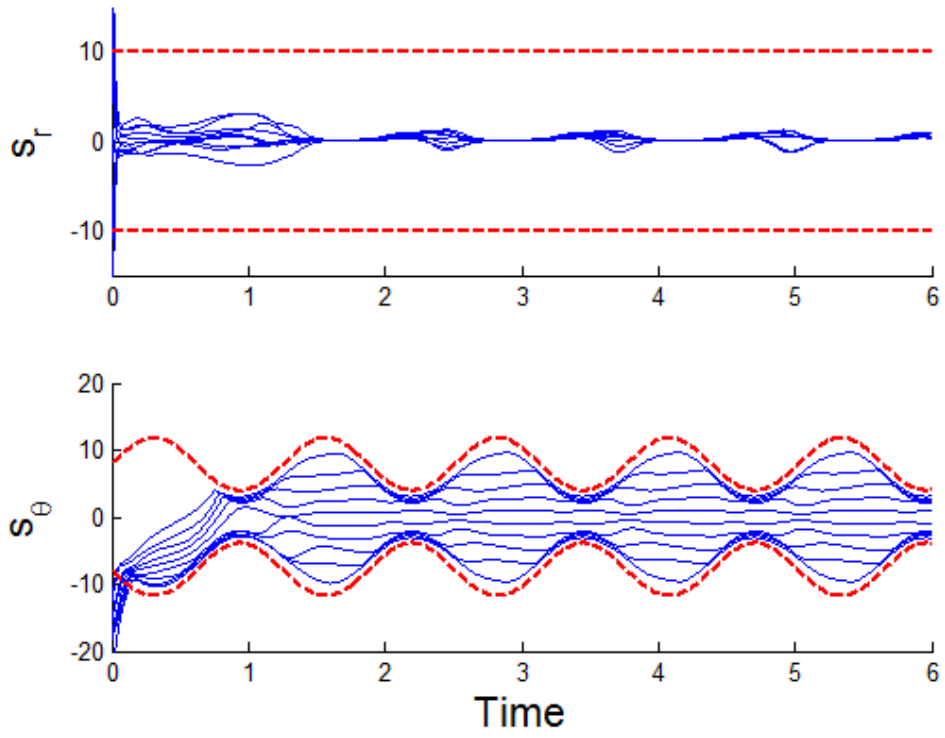

FIGURE 19: Sliding functions of all agents in Case Study 4

We see in Figure 18 that the agents are quickly driven into the region, as expected. One especially interesting element to note in this simulation as opposed to the circular and elliptical cases is our selection of a time varying boundary layer in the angular direction. Figure 19 shows that the boundary layer (represented by a red dashed line) is varying harmonically in the angular direction. This in turn prevents a true steady state for the agents, however we do see that all the sliding functions remain entrapped. The selection of λ reduces the impact of the derivative term, and allows us to claim nearly robust region tracking. Additionally, we observe a relatively even distribution of the sliding vectors within the boundary layer.

4. APPLICATIONS IN HERDING

The RHSMC discussed in Section 3 was initially conceived as a method to position controlled agents ('*pursuers*') in a decentralized fashion to form elliptical 'paddles'. These paddles were formed with the intent of creating a front of agents which would cause herding behavior in another group of agents ('*evaders*'). Additionally, a second method of herding was developed using the same control concept, modified to accommodate an arc shaped region. Both implementations start from the same jumping off point of calculating the feedback control repulsions which will lead to stable evader tracking of a desired trajectory.

Note that although the RHSMC is capable of dealing with additional unknown forces and unmodeled dynamics (provided bounds are available for both), we do not utilize this feature in our herding analysis for simplicity. We restrict the unknown forces to consist solely of the pursuer-on-pursuer repulsions.

The pursuer dynamics are written as a simplified version of Equation (1),

$$m_p \ddot{\mathbf{z}}_j + b_p \dot{\mathbf{z}}_j = \mathbf{f}_j^r(W_j) + \mathbf{u}_j \in \Re^2 \qquad j = 1, 2, ..., M \qquad (49)$$

where $\mathbf{z}_j \in \Re^2$ remains the position of the j^{th} pursuer with mass and drag coefficients m_p and b_p.

Sections 4.1 and 4.2 will develop the evader dynamics and determine a feedback force which the herders will apply. Sections 4.3 and 4.4 generate control logic for a 2v1 and MvN case respectively which will utilize the ellipse RHSMC developed in 3.2. Sections 4.5 and 4.6 will introduce a cylindrical coordinate

variant of RHSMC herding which greatly simplifies the problem in both 2v1 and MvN cases.

4.1 EVADER DYNAMICS

We consider an evader swarm of agent count *N*. The dynamics are given

$$m_e\ddot{\mathbf{y}}_i + b_e\dot{\mathbf{y}}_i = \sum_{j\in W_{p,i}}\mathbf{f}_{ep,i,j} + \sum_{k\in W_{e,i}}\mathbf{f}_{ee,i,k} \qquad i = 1, 2, ..., N \tag{50}$$

where $\mathbf{y}_i \in \Re^2$ is the position of the i^{th}. m_e and are the mass and drag coefficients respectively. The forces $\mathbf{f}_{ep,i,j}$, $\mathbf{f}_{ee,i,k}$ are interaction forces between two agents. $\mathbf{f}_{ep,i,j}$ is the pursuer to evader repulsion force, which is felt by the i^{th} evader due to the j^{th} pursuer

$$\mathbf{f}_{ep,i,j} \equiv \rho\cdot\left(r_e - \left\|\mathbf{y}_i - \mathbf{z}_j\right\|\right)\cdot\hat{\mathbf{v}}_{\mathbf{y}_i,\mathbf{z}_j} \tag{51}$$

An example of this force profile is shown in Fig. 20. This force is non-zero only when pursuer-evader distance is less than *evader sensing range*, r_e. The parameter ρ is an amplification parameter.

$\mathbf{f}_{ee,i,k}$, is the interaction force felt by the j^{th} evader due to the k^{th} evader, and it is modeled with similar properties as the interactions in [5] as

$$\mathbf{f}_{ee,i,k} \equiv \frac{\alpha-\beta\left\|\mathbf{y}_i-\mathbf{y}_k\right\|}{1+\gamma\left\|\mathbf{y}_i-\mathbf{y}_k\right\|}\hat{\mathbf{v}}_{\mathbf{y}_i,\mathbf{y}_k} \tag{52}$$

It is depicted in Fig. 21 for a sample parameter set given in Table 3 (borrowed from the example section). This force represents repulsion at short range and an attraction at long range with an equilibrium distance between them. Similar force profiles are suggested in [3] as being biologically inspired interactions which

create stable swarming behavior. The parameters α, β and γ control the profile shape; α is the maximum repulsive force when $\|\mathbf{y}_i - \mathbf{y}_k\| = 0$, the equilibrium $\left(\|\mathbf{f}_{ee,i,k}\| = 0\right)$ distance is $\|\mathbf{y}_i - \mathbf{y}_k\| = \alpha / \beta$, and the maximum attractive force, β / γ, occurs at infinite distance.

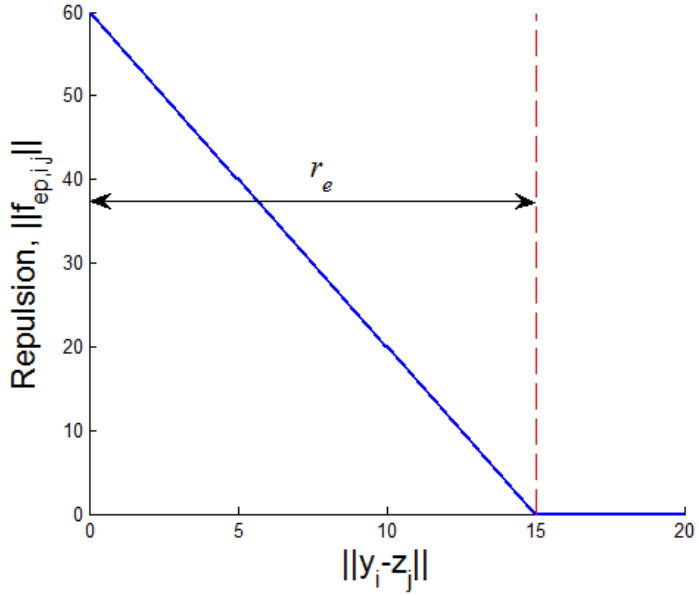

FIGURE 20: $\mathbf{f}_{ep,i,j}$ repulsive force profile

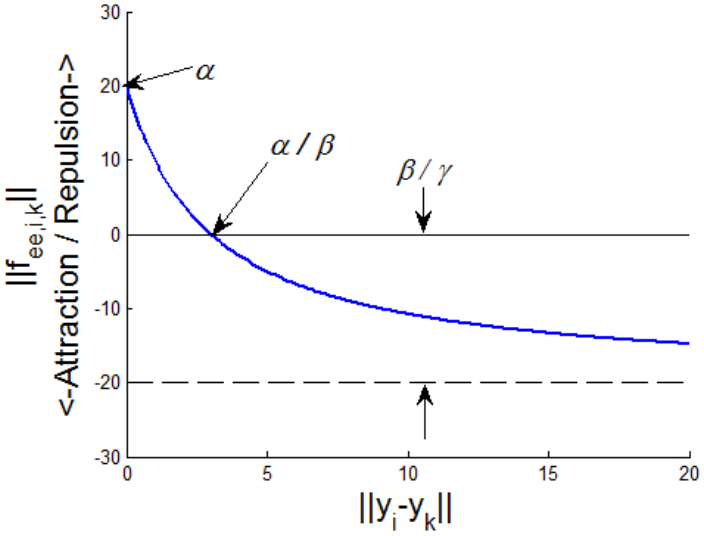

FIGURE 21: $\mathbf{f}_{ee,i,k}$ interaction force profile

We define the centrode of the evader swarm and write its dynamics,

$$\bar{\mathbf{y}} = \frac{1}{N}\sum_{i=1}^{N}\mathbf{y}_i \tag{53}$$

$$m_e\ddot{\bar{\mathbf{y}}} + b_e\dot{\bar{\mathbf{y}}} = \frac{1}{N}\sum_{i=1}^{N}\sum_{j=1}^{M}\mathbf{f}_{ep,i,j} \tag{54}$$

Note that $\frac{1}{N}\sum_{i=1}^{N}\sum_{\substack{k=1\\k\neq i}}^{N}\mathbf{f}_{ee,i,k} = 0$, because every evader pair has an equal and opposite interaction.

4.2 EVADER HERDING FORCE

It is evident in Equation (54) that the evader's centrode dynamics are governed only by the repulsion forces from the pursuers. In order to guide the evader along a desired trajectory, $\mathbf{y}_d(t)$, also known as "herding", we need to deploy a nominal feed forward herding force on the evader, $\mathbf{f}_d$.

$$m_e\ddot{\mathbf{y}}_d + b_e\dot{\mathbf{y}}_d = \mathbf{f}_d \tag{55}$$

Pursuant to our stated goal of minimizing the distance between the evader's centrode and the desired trajectory, and to study the trajectory tracking and disturbance rejection capabilities, we define an evader error

$$\mathbf{e}_e = \bar{\mathbf{y}} - \mathbf{y}_d \tag{56}$$

to be minimized.

Here we make a critical assumption that the total repulsive force felt by the evader swarm centrode is approximately equal to the force that would be felt if all evaders were lumped at the centrode. That is, $\frac{1}{N}\sum_{i=1}^{N}\sum_{j=1}^{M}\mathbf{f}_{ep,i,j} = \sum_{j=1}^{M}\mathbf{f}_{ep,j}$.

Combining Eqs. (30-32), one obtains the evader error dynamics as

$$m_e\ddot{\mathbf{e}}_e + b_e\dot{\mathbf{e}}_e = \sum_{j=1}^{M}\mathbf{f}_{ep,j} - \mathbf{f}_d = \mathbf{f}^* - \mathbf{f}_d \tag{57}$$

where $\mathbf{f}^*$ is the self evident summation term, which is called the *herding force* in the remainder of the text. Notice that $\mathbf{f}^* = \mathbf{f}_d + m_e\ddot{\mathbf{e}}_e + b_e\dot{\mathbf{e}}_e$ is the combined feed forward force and the error compensating terms.

In order to ensure asymptotically stable tracking, we suggest the following PD-type structure for $\mathbf{f}^*$

$$\mathbf{f}^* \equiv -P_e\mathbf{e}_e - D_e\dot{\mathbf{e}}_e + \mathbf{f}_d \tag{58}$$

where $P_e, D_e > 0$ are the feedback gains. The '*e*' subscript indicating that these control gains are relevant to the evader. This selection brings Equation (57) to

$$m_e\ddot{\mathbf{e}}_e + (b_e + D_e)\dot{\mathbf{e}}_e + P_e\mathbf{e}_e = 0 \tag{59}$$

of which the poles (p_1, p_2) are obtained from the characteristic equation

$$m_e s^2 + (b_e + D_e)s + P_e = 0 \tag{60}$$

In this study, we select the P_e and D_e gains such that both characteristic roots are negative real.

Having established this control scheme the main objective of herding reduces to the task of properly positioning the pursuers to create the given herding force, $\mathbf{f}^*$, while the pursuers (herders) have limited knowledge of the positions (and consequently repulsive forces) of the other pursuers. This is the focus of the control and main development in the application portion of this thesis.

4.3 PADDLE BASED HERDING IN THE 2v1 CASE

In preparation for the more advanced scenario with larger groups of evaders and pursuers we first take $N = 1$, $M = 2$. This simplifies a good deal of the analysis, especially for the method presented in 4.3 and 4.4. To create the herding force, $\mathbf{f}^*$, we need to select desired pursuer positions. These positions can only be generated if the herding force is bounded by $\|\mathbf{f}^*\| \le 2\rho r_e = \|\mathbf{f}^*\|_{peak}$ from Equation (51). Intuition states that two pursuers would have a significant advantage compared to single pursuer trying to herd an evader along a desired path.

Ideally the 2 pursuers will be symmetric vis-à-vis $\mathbf{f}^*$. A pair of example positions is shown in Fig. 22. These ideal positions described by a distance and an angle, r_d and $\theta_d \pm \Delta\theta$.

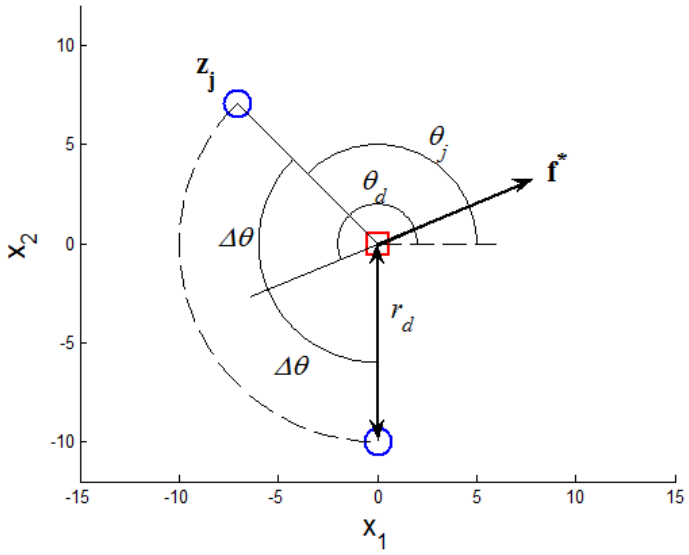

FIGURE 22: Illustrating the desired pursuer positions

The pursuer positions at which the agents jointly execute the force **f*** on the evader, are stated as

$$\mathbf{z}_{d2,j} = \mathbf{y} - r \cdot \mathbf{R}(\pm \Delta\theta) \cdot \frac{\mathbf{f}^*}{\|\mathbf{f}^*\|} \qquad j=1,2 \tag{61}$$

The subscript *d*2 indicates that this is the desired position during control phase 2 (explained in depth shortly). $\mathbf{R}(\Delta\theta) \in \Re^{2\times 2}$ is the right handed rotation matrix by angle $\Delta\theta$. The selection of r_d and $\Delta\theta$ is not unique and in this section we use the following heuristic method to generate them. Combining Eqs. (51) and (58) we state that

$$\|\mathbf{f}^*\| = 2\rho(r_e - r_d)\cos(\Delta\theta) \tag{62}$$

The maximum value for r_d capable of producing a given $\mathbf{f}^*$ is $r_{max}(\mathbf{f}^*) = r_e - \frac{\|\mathbf{f}^*\|}{2\rho}$ and it occurs when $\Delta\theta = 0$. We invite a separation angle, $\Delta\theta$, by limiting the distance r_d to be smaller than $r_{max}(\mathbf{f}^*)$ by a certain fraction χ.

$$r_d = \chi r_{\max} = \chi\left(r_e - \frac{\|\mathbf{f}^*\|}{2\rho}\right) \qquad 0 << \chi < 1 \tag{63}$$

For all the work in this text we utilize $\chi = 0.95$. Solving Equation (62) with (63) for the required angle,

$$\Delta\theta = \cos^{-1}\left(\frac{\|\mathbf{f}^*\|}{2\rho(r_e - r_d)}\right) \tag{64}$$

Figure 23 shows the loci of pursuer positions for varying magnitudes of force, $0 \le \|\mathbf{f}^*\| \le \|\mathbf{f}^*\|_{peak}$. Notice that the force line of action is taken horizontal and both directions are considered.

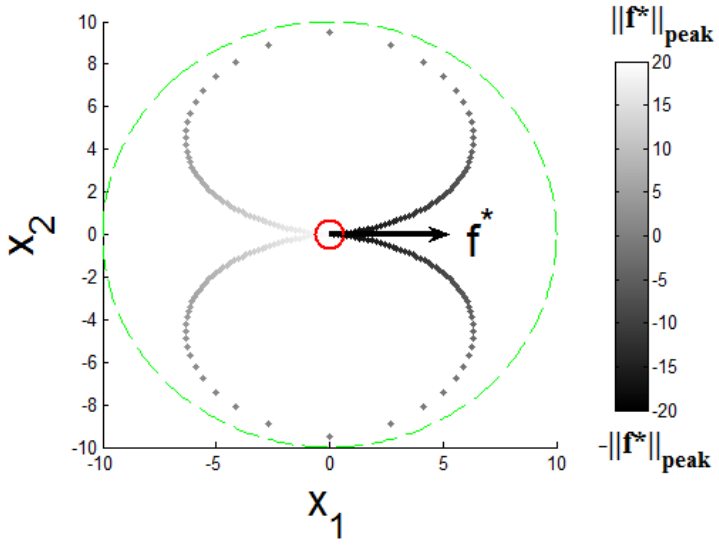

FIGURE 23: Loci of pursuer positions for varying magnitudes of $\mathbf{f}^*$ with $\chi = 0.95$, $\rho = 1$, $r_e = 10$ (shown as a green dashed line)

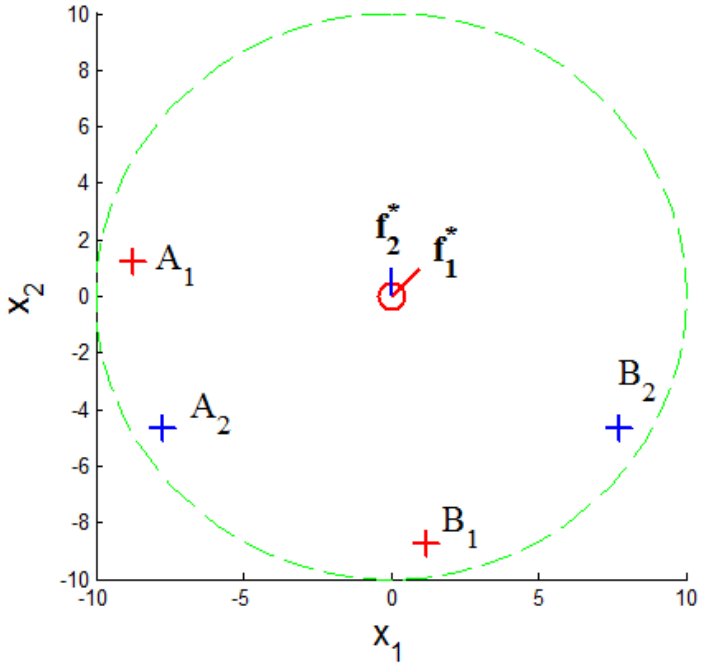

FIGURE 24: Small changes in the herding force lead to rapid rotations of desired herding positions

If the vector $\mathbf{f}^*$ becomes small, any slight disturbance may change its direction substantially (as much as 90 degrees). This in turn results in rapid motion of the pursuers' positions according to the heuristic scheme above (see points A_1, B_1 move to A_2, B_2 to accommodate the small change from $\mathbf{f}_1^*$ to $\mathbf{f}_2^*$ in Fig. 24)

These motions are most exaggerated when the herding force amplitude is small and so we propose a dead-zone nonlinearity to the force direction variations. If the force amplitude drops below 5% of the maximum repulsion possible from the two agents as declared by Equation (51), $\left\|\mathbf{f}^*\right\| < 0.05 \cdot 2 \cdot \max\left(\mathbf{f}_{ep,i,j}\right) = 0.1\rho r_e$, we set the direction of the small herding force to point to the ultimate target, i.e., $\frac{\mathbf{f}^*}{\left\|\mathbf{f}^*\right\|} = \hat{\mathbf{v}}_{\mathbf{y}_f, \bar{\mathbf{y}}}$ where $\mathbf{y}_f$ is the final desired position. When the herding force increases sufficiently (beyond 10% of the maximum repulsion from both agents), its direction is again determined using Equation (58). Additionally we implement a first order filter over $\angle\mathbf{f}^*$ (with a pole p_3) which assists in the transition between these two regimes.

A heuristic scheme of controlling the pursuers is suggested, having three phases, each addressing a specific segment of the task.

Phase 1, the **alignment phase**, where the pursuers are maneuvered around the evader outside its sensing range. The objective is to bring the pursuers (without influencing the evader) to two staging positions which are appropriate for initiating the herding. These positions are typically on the opposite side of the evader as the target location. We denote the control action for this phase as $\mathbf{u}_{j,1}$.

Phase 2, the **herding phase**, where the pursuers track the desired positions of Equation (61) as prescribed by the forcing given in Equation (34). The corresponding control action for this phase is $\mathbf{u}_{j,2}$.

Phase 3, the **containment phase**, in which the pursuers move out of the evader sensing range and maintain zero herding force. They are positioned to intervene if the evader departs from the desired target location and Phase 1 action is re-triggered. The control in this phase is $\mathbf{u}_{j,3}$.

The superposition of three control elements creates the total control effort

$$\mathbf{u}_j = a_1\mathbf{u}_{j,1} + a_2\mathbf{u}_{j,2} + a_3\mathbf{u}_{j,3}, \qquad a_1, a_2, a_3 \in Z, \quad a_1 + a_2 + a_3 = 1 \tag{65}$$

where Z represents binary numbers. This formulation makes only one phase active at any given instant. However, abrupt phase transitions are not desirable as it would introduce discontinuities in control effort. Therefore the binary numbers in Equation (65) are slightly modified to introduce ramp-type transitions between the two adjacent phases. This is achieved by linearly decreasing the control from the old phase while linearly increasing the control force from the new phase over a predetermined duration, Δt_{phase}. Figure 25 illustrates the method with a 1 second transition time.

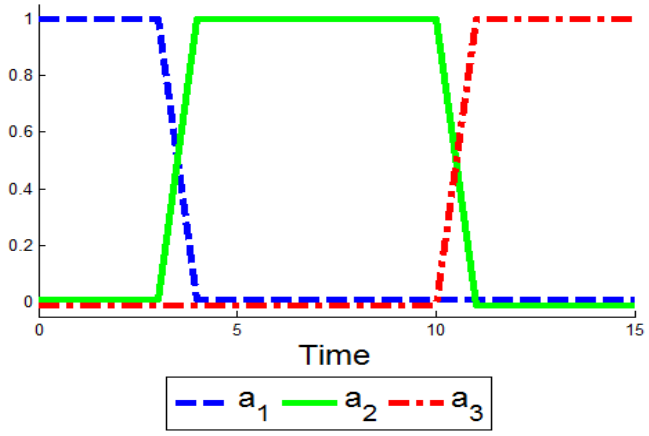

FIGURE 25: Transition from phase 1 to 2 starting at $t = 3$,

and from phase 2 to 3 starting at $t = 10$

In this reduced 2v1 scenario, the form of the controller is identical between phases, but each phase has unique desired trajectories. We will develop the controller below independent of the trajectories, by defining a general error

$$\mathbf{e}_{p,j} = \mathbf{z}_j - \mathbf{z}_{d,j} \tag{66}$$

We then write our desired pursuer dynamics,

$$m_p \ddot{\mathbf{z}}_{d,j} = \mathbf{f}_{d,j} \tag{67}$$

Investigating the error dynamics and determining our control action in a similar manner to Eqs. (57) and (58),

$$m_p \ddot{\mathbf{e}}_{p,j} = \mathbf{u}_{j,1} + \sum \mathbf{f}_{pp} - \mathbf{f}_{d,j} \tag{68}$$

$$\mathbf{u}_j \equiv b_p \dot{\mathbf{z}}_j + m_p \left[\ddot{\mathbf{z}}_{d,j} - P_p \mathbf{e}_{p,j} - D_p \dot{\mathbf{e}}_{p,j} \right] \tag{69}$$

This control leads to the final error dynamics

$$\ddot{\mathbf{e}}_{p,j} + D_p \dot{\mathbf{e}}_{p,j} + P_p \mathbf{e}_{p,j} = \sum \mathbf{f}_{pp} \tag{70}$$

which is an attenuation filter over the disturbance force composition given in the summation. The subscript 'p' in the control gains indicates that these are acting in the pursuer control. The characteristic equation is,

$$s^2 + D_p s + P_p = 0 \tag{71}$$

The control gains in Equation (69), P_p and D_p, are selected to create negative real roots in Equation (71), p_4 and p_5, again for non-oscillatory decay in the approach. Note that using the same PD control gains in all of the three phases will (desirably) bring about identical rates of pursuer error decay.

Phase 1 – Alignment, $\mathbf{u}_{j,1}$, $\mathbf{z}_{d1,j}$

The phase one control, $\mathbf{u}_{j,1}$ operates according to the scheme in Equation (68), on the error

$$\mathbf{e}_{p1,j} = \mathbf{z}_j - \mathbf{z}_{d1,j} \tag{72}$$

In this phase the pursuers are maneuvered starting from their initial distributions towards two target positions where they can execute the calculated initial herding force $\mathbf{f}^*(t=0)$ as per Equation (61). By careful selection of the trajectories and end configuration of this phase, they execute no herding force. We use a 20% buffer beyond the evader's sensing radius, r_e, as the safe radius in determining the final configuration, by selecting

$$r_{safe} = 1.2 \cdot r_e \tag{73}$$

The desired pursuer positions at the end of phase 1 are shown in Fig. 26,

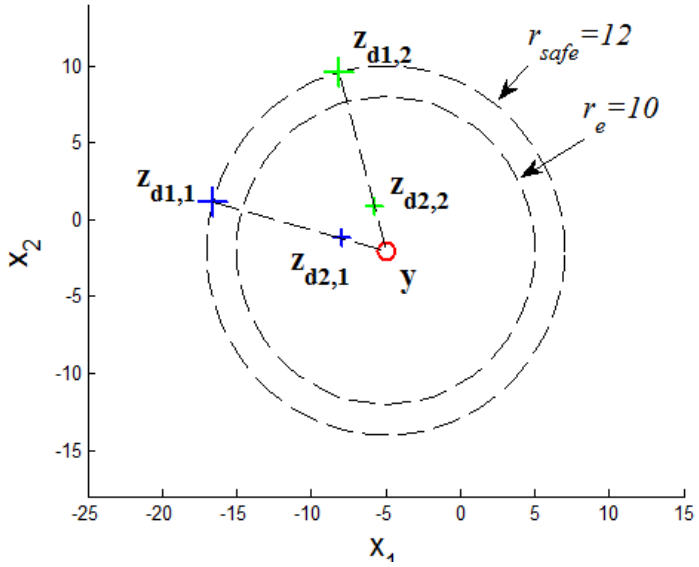

FIGURE 26: Phase 1 final desired positions

In order to bring the pursuers to these positions, we look at the vectors connecting $\bar{\mathbf{y}}$ to $\mathbf{z}_j$, defined by its magnitude, r_j, and angle, θ_j,

$$\mathbf{z}_j = r_j\left[\cos(\theta_j) \quad \sin(\theta_j)\right]^T + \bar{\mathbf{y}} \qquad j = 1, 2 \tag{74}$$

We propose a desired behavior for this vector,

$$\mathbf{z}_{d1,j}(t) = r_{d,j}\left[\cos(\theta_{d,j}) \quad \sin(\theta_{d,j})\right]^T - \bar{\mathbf{y}}(t=0) \qquad j = 1, 2 \tag{75}$$

with the selection of

$$r_{d,j}(t) = (r_{j0} - r_{safe})e^{-p_4 t} + r_{safe} \tag{76}$$

$$\theta_{d,j}(t) = \left(\theta_{j0} - \angle\hat{\mathbf{v}}_{\mathbf{z}_{d2,j},\bar{\mathbf{y}}}(t=0)\right)e^{-p_4 t} + \angle\hat{\mathbf{v}}_{\mathbf{z}_{d2,j},\bar{\mathbf{y}}}(t=0) \tag{77}$$

This selection indicates both a radial and angular decay, as can be seen in Fig. 27.

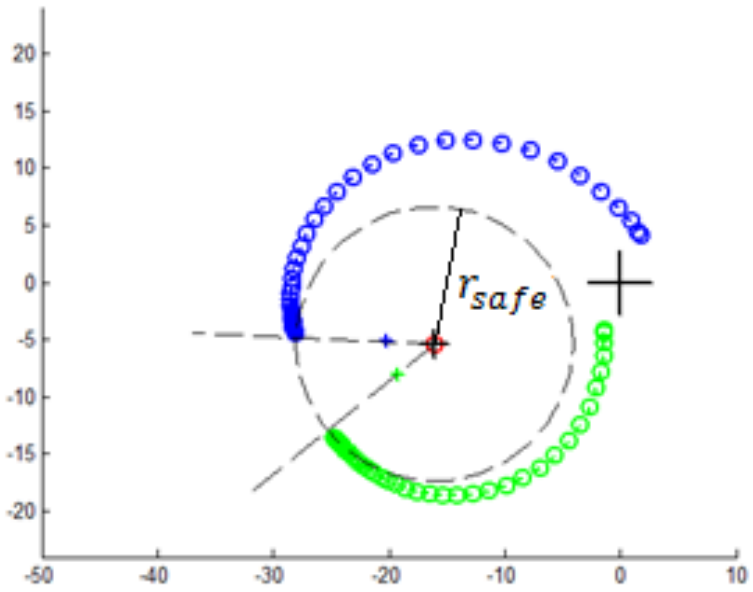

FIGURE 27: Phase 1 time trace for a stationary evader

Because we are selecting the desired final Phase 1 pursuer positions under the assumption of a stationary evader, we note the following limitation: a moving evader may be capable of feeling influence from the pursuers if

$$\left\|\dot{\bar{\mathbf{y}}}\right\| \geq 0.2 \cdot r_e / t_1 \tag{78}$$

where $t_1 = 4/p_4$ corresponds to 4 time constants of the pursuer error dynamics and the decay of the exponential elements in the desired vector. We restrict our analysis to cases in which this condition is never true during Phase 1.

We note that the pursuer-pursuer forces are left untouched by the controller. As we anticipate the agents moving to separate staging areas, this force is expected to be small.

The final position for this phase is given as

$$\mathbf{z}_{d1,j}(t_1) \approx \bar{\mathbf{y}} + r_{safe}\mathbf{v}_{\mathbf{z}_{d2,j},\mathbf{y}}(t=0) \qquad j = 1, 2 \tag{79}$$

We state that the phase is completed when

$$t = t_1 = 4 / p_4 \tag{80}$$

Phase 2 – Herding, $\mathbf{u}_{j,2}$, $\mathbf{z}_{d2,j}$

In the herding phase, we wish to apply $\mathbf{f}^*$, and so we define our desired positions via Equation (61-64). The error used by the controller is then,

$$\mathbf{e}_{p2,j} = \mathbf{z}_j - \mathbf{z}_{d2,j} \qquad j = 1,2 \tag{81}$$

This phase is completed when the *evader* is sufficiently close to the FINAL target, $\mathbf{y}_f$, with sufficiently small relative velocity, as determined by the end user's requirements.

$$\left\| \bar{\mathbf{y}} - \mathbf{y}_f \right\| < \psi_1, \qquad \left\| \dot{\bar{\mathbf{y}}} - \dot{\mathbf{y}}_f \right\| < \psi_2 \tag{82}$$

Phase 3 - Containment, $\mathbf{u}_{j,3}$, $\mathbf{z}_{d3,j}$

The goal of Phase 3 is to push the pursuers back to the safe radius. This prevents them from unnecessarily disturbing the evader. We apply the same control as Phases 1 and 2, but with the desired positions selected as

$$\mathbf{z}_{d3,j} = \bar{\mathbf{y}} - r \cdot \mathbf{R}\left(\pm \tfrac{\pi}{2}\right) \cdot \hat{\mathbf{v}}_{\mathbf{y}(t=0),\mathbf{y}_f} \qquad j=1,2 \tag{83}$$

This positions the pursuers opposite each other at a constant angle.

SUMMARY OF CONTROL LOGIC FOR 2v1

In order to achieve the herding presented here, the following steps are taken in the implementation of the control.

1: Calculate the herding force, $\mathbf{f}^*$ Equation (58)

2: Calculate desired positions for the pursuers which generate this force, $\mathbf{z}_{d2,1}, \mathbf{z}_{d2,2}$ Equation (61)

3: Apply 3-phase control logic on pursuers Equation (65)

with unique desired trajectories for

Phase 1: Alignment Equation (75)

Phase 2: Herding through repulsion Equation (61)

Phase 3: Containment Equation (83)

A crucial point of robustness is the disruption in the sequence 1-2-3 above. In any instant, if the pursuers notice the evaders' behavior is calling for an earlier phase, the strategy should revert and pursue the sequence again. For instance while in Phase 2 if the evader makes a significant transverse directional move due to a disturbance, Phase 1 realignment may be required. Another situation would significant evader motion in Phase 1. In that case desired trajectories of the pursuers have to be updated and Phase 1 may need to be performed again. For brevity, we restrict the coverage to cases which Equation (78) is never true, and illustrate only marginal disturbances on the evader.

In order for the pursuers to successfully perform the herding their error dynamics must be significantly faster than the evaders'. Recall that p_1, p_2 are

related to the evader error dynamics, p_3 is the filter pole for the angle, and p_4 and p_5 are related to the pursuer error dynamics. Both the filter and the pursuer dynamics must be faster than the evader control logic and we state,

$$p_1 > p_2 >> p_3 \geq p_4 > p_5 \in \Re^- \tag{84}$$

We call this herding method quasi-decentralized to indicate that portions of the process require universal knowledge (calculation of the desired repulsive forces on evaders and the ideal pursuer positions) but we have seen that the individual pursuers act solely based on their desired trajectories for the given phase and local interactions.

CASE STUDY 5: 2v1 Ellipse Based Herding

For Case Study #5, the evaders are herded on a decaying desired trajectory, $\mathbf{y}_d(t) = (\mathbf{y}_{t=o} - \mathbf{y}_f)e^{-\kappa t} + \mathbf{y}_f$ using the parameters found in Table 3. The poles are selected as $p_1 = -1, \quad p_2 = -2, \quad p_3 = -10, \quad p_4 = -10, \quad p_5 = -12$. The evader has a small nonzero initial velocity, and receives a moderate impulsive disturbance at time *t=1.5*.

Evader Control

$m_e = 4.0$	$m_p = 1.0$	$\mu = 10$	$\chi = 0.95$
$b_e = 1.0$	$b_p = 1.0$	$r_p = 4$	$\psi_1 = 1.0$
$\rho = 10$	$\mathbf{y}_f = [0,0]$	$\kappa = 0.4$	$\psi_2 = 0.3$
$r_e = 10$	$P_e = 8$	$D_e = 11$	$t_1 = 0.4$
	$P_p = 120$	$D_p = 22$	$\Delta t_{phase} = 0.1$
	$p_3 = -10$		

TABLE 3: Parameters for Case Study 5

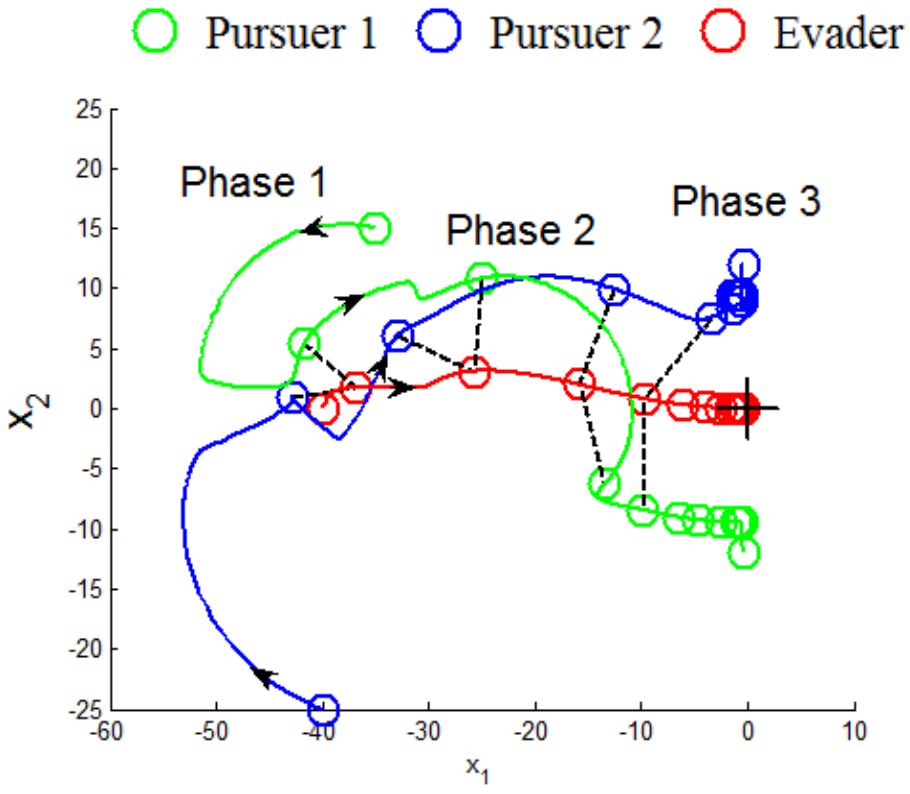

FIGURE 28: Time trace of Case 5

The circular icons are spaced at 1 second intervals. We can see in Fig. 25 that the evader (in red) initially lies on the x_1 axis, with a small initial velocity. At time $t = 1.5$ seconds, an impulsive disturbance effects the evader, and the pursuers which initially would have passed around both sides of the evader now move to apply control action in the vertical direction as well. At the end of the simulation, we see the pursuers move away from the evader, which lies stationary at the origin.

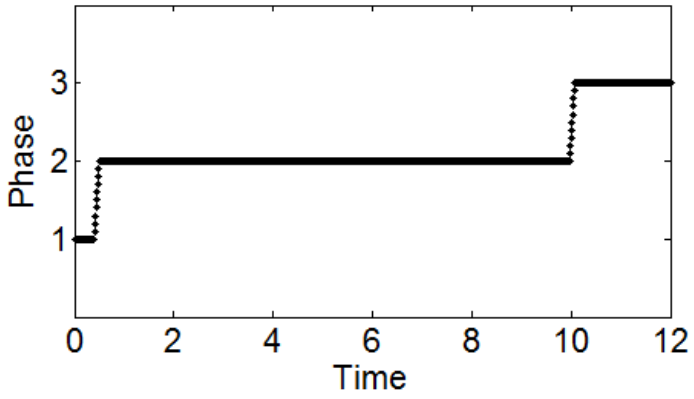

FIGURE 29: Control Phase

Figure 29 shows the time history of the control phase. As prescribed, Phase 1 is resolved after $t_1 = 0.4$ seconds. Phase 3 is triggered when the herding operation is complete, and its length is determined by the decay rate of the desired evader trajectory.

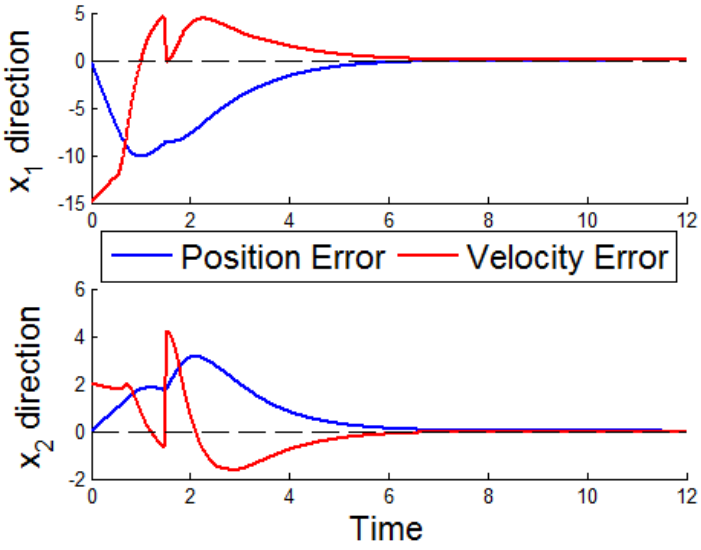

FIGURE 30: Evader Error

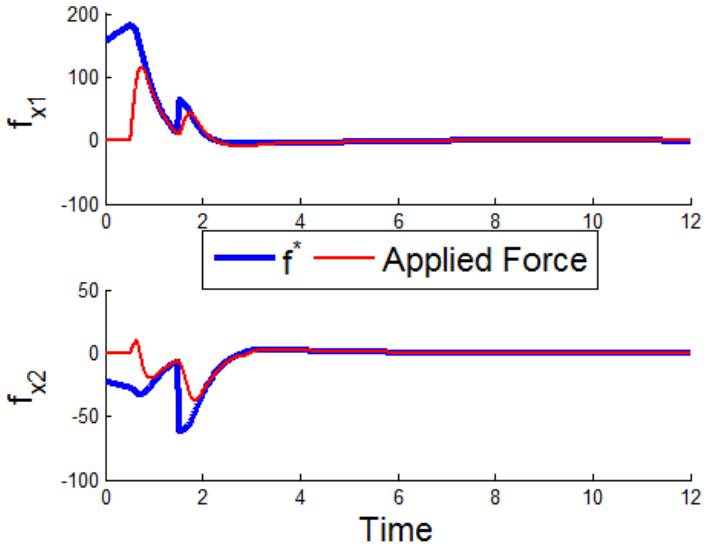

FIGURE 31: Evader Control Forces

Figure 30 shows the evader's error. We note the step in velocity error related to the impulse at 1.5 seconds, and that following this, the error decays in

an additional 4 time constants of the evader error dynamics (4 seconds from $4/p_1$). Figure 31 shows the calculated feedback herding force, as well as the force applied by the pursuer's repulsion. In the x_2 direction, there is a small unhelpful application of force just after t_1. This is an effect of the initial velocity of the evader, which is not accounted for during Phase 1. It is quickly corrected as the feedback control calculates new Phase 2 desired positions which the agents track, bringing the applied force to match the requested herding force, $\mathbf{f}^*$.

4.4 PADDLE BASED HERDING IN THE MvN CASE

In order to accommodate more agents in both groups, we investigate several additions. The pursuer swarm is divided into two equal-strength subgroups, and we utilize similar logic to the 2v1 scenario by using the centrodes of each of the three groups as if they were lumped single-agent entities.

We split the pursuers into two separate groups of strength *M*/2, with the respective centrodes

$$\bar{\mathbf{z}}_\ell = \tfrac{2}{M}\sum_{j\in R_\ell}\mathbf{z}_j \qquad \ell = 1, 2 \tag{85}$$

where R_ℓ contains the indices of agents in each group, and disjoint sets $R_1 \cup R_2 = \{1,2,...,M\}$. The dynamics of these centrodes are

$$m_p\ddot{\bar{\mathbf{z}}}_\ell + b_p\dot{\bar{\mathbf{z}}}_\ell = \tfrac{2}{M}\sum_{j\in R_\ell}\sum_{\substack{k=1\\k\neq j}}^{M}\mathbf{f}_{pp,j,k} + \tfrac{2}{M}\sum_{j\in R_\ell}\mathbf{u}_j \tag{86}$$

The similarity of the centrode dynamics in Eqs. (86) and (54) to the original agent dynamics in Eqs. (1) and (50) is obvious and motivates this direct extension of the 2v1 logic.

We expand the pursuer positioning logic of Equation (63-64), with the assumption that the forces applied by pursuers evenly distributed about the desired centrode produces $M/2$ times the force produced by each single pursuer in the 2v1 scenario,

$$r_d = \chi\left(r_e - \frac{\|\mathbf{f}^*\|}{M\rho}\right) \qquad 0 << \chi < 1 \tag{87}$$

$$\Delta\theta = \cos^{-1}\left(\frac{\|\mathbf{f}^*\|}{M\rho(r_e - r)}\right) \tag{88}$$

The desired staging areas utilized in Phase 1 and the final positions of Phase 3 are dependent on the evaluation of a safe radius. As the evader swarm now has appreciable geometric spread, we should include this in our analysis and be sure to move the pursuers outside the sensitivity zone of all of the evaders (during Phases 1 and 3).

$$r_{safe} = 1.20 \cdot \left[r_e + \max\left(\|\mathbf{y}_i - \bar{\mathbf{y}}\|\right)\right] \tag{89}$$

In phase 2, the radius and shape of each group of pursuers is important to monitor. By utilizing the results of section 3 to instate a region tracking controller, we can ensure the agents are adequately contained in elliptical '*paddles*'. The benefit of using an elliptical configuration is that we create a more even front of applied force rather than a single point source.

The desired centrodes, $\bar{\mathbf{z}}_{d,\ell}$, are generated similarly to the 2v1 case. The job of the sliding mode controller is to ensure that the vector $\mathbf{s}_j$ is driven to zero, at which time Equation (5) indicates a first order exponential decay of the pursuer

error. The controller is given as a direct implementation of Equation (16) in the case of no parameter uncertainty.

$$\mathbf{u}_{j,2} \equiv b_p \dot{\mathbf{z}}_j - m_p \left[\lambda\left(\dot{\mathbf{z}}_j - \dot{\bar{\mathbf{z}}}_{d,\ell}\right) - \ddot{\bar{\mathbf{z}}}_{d,\ell} + K_1 \mathbf{s}_j + K_2 \mathrm{sat}\left(\mathbf{s}_j\right) \frac{\mathbf{s}_j}{\|\mathbf{s}_j\|} \right] \tag{90}$$

The control is robustizing if the K_2 gain is greater than the magnitude of the uncertain pursuer-on-pursuer repulsion terms, $K_2 \mathrm{sat}\left(\mathbf{s}_j\right) > \left\| \frac{1}{m_p} \sum_{\substack{k=1 \\ k \neq j}}^{M} \mathbf{f}_{pp,j,k} \right\|$. This indicates a decay of $\mathbf{s}_j$ and ultimately a decay of the pursuer error. Traditionally, the boundary layer is utilized to smooth the transition of $\mathbf{s}_j$ from positive to negative. In our scenario, we use the boundary layer to intentionally compromise the robust nature of the controller. This leads to a manageable error in position which allows the agents to distribute themselves inside a geometric region.

Further, by selecting K_1 and λ as

$$K_1 \lambda = P_p, \qquad K_1 + \lambda = D_p \tag{91}$$

Equation (90) can be re-written to correspond to the gain values of the other phases,

$$\mathbf{u}_{j,2} \equiv b_p \dot{\mathbf{z}}_j - m_p \left[P_p\left(\mathbf{z}_j - \bar{\mathbf{z}}_{d,\ell}\right) + D_p\left(\dot{\mathbf{z}}_j - \dot{\bar{\mathbf{z}}}_{d,\ell}\right) - \ddot{\bar{\mathbf{z}}}_{d,\ell} + K_2 sat\left(\mathbf{s}_j\right) \frac{\mathbf{s}_j}{\|\mathbf{s}_j\|} \right] \tag{92}$$

Therefore, the Phase 2 control will retain similar time constants as in the previously illustrated method. The sole difference is the robustizing force of K_2.

The oblique angle of the ellipse is updated at regular low frequency intervals so that the minor axis is directed towards the evader swarm's center. This

smoothes the repulsive forces into a front which assists in containing the evader swarm. The updates to the angle can be seen as impulsive disturbances, which SMC effectively rejects.

Expected outcome of SMC deployment on the pursuer swarms is that their centrodes will follow a trajectory as in 2v1. Having the pursuer agents robustly distributed in the ellipses which are formed around these centrodes, as described above, they will act like *paddles* to herd the evaders towards the target region.

Here we present two simulations of the above control sequence. In the first, two pursuers push a single evader to a final position. The second simulation illustrates multiple evaders herded by multiple pursuers along a circular trajectory.

CASE STUDY 6: MvN Ellipse Based Herding

In order to illustrate the effectiveness of the proposed control in a multi-agent environment, we use 10 pursuers to herd 20 evaders along a circular path, with desired trajectory, $\mathbf{y}_d(t) = 10 \cdot [\sin(t), \quad -\cos(t)]^T$ and parameters listed in Table 4.

Evader Control

$m_e = 4.0$	$m_p = 1.0$	$\mu = 100$	$\chi = 0.95$
$b_e = 1.0$	$b_p = 1.0$	$r_p = 4$	$\psi_1 = 1.0$
$\rho = 4$	$P_e = 8$	$D_e = 11$	$\psi_2 = 0.3$
$r_e = 15$	$P_p = 120$	$D_p = 22$	$t_1 = 0.4$
$\alpha = 20$	$K_2 = 593$	$\Delta t_{phase} = 0.1$	$p_3 = -10$
$\beta = 20/3$	$major = 4$		
$\gamma = 1/3$	$minor = 2$		

TABLE 4: Parameters for Case Study #6

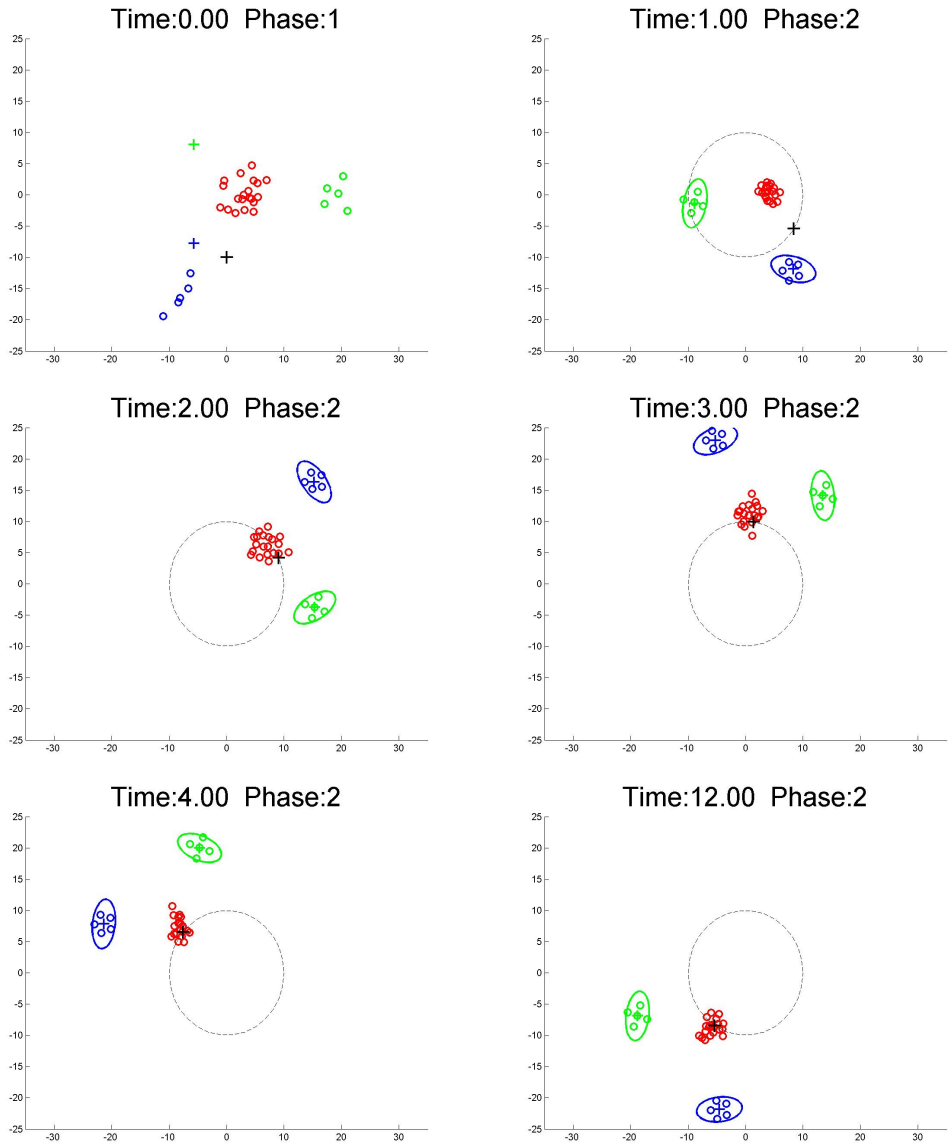

FIGURE 32: Snapshots of case study 5 at $t = 0, 1, 2, 3, 4, 12$ seconds

Due to the more complex nature of the MvN scenario, we illustrate the methods effectiveness through snapshots of the simulation. For this simulation, the evader centrode has a zero initial velocity. The pursuers expectedly enter Phase 2 at t_1, and can be seen herding by the second snapshot. Between 1 and 4

seconds, we see a drastic reduction in the evader error both in Figs. 29 and 30. The small oscillating error seen in Figure 33 after the expected decay is due to the innaccuracy in application of the herding force. This can be seen in Figure 31.

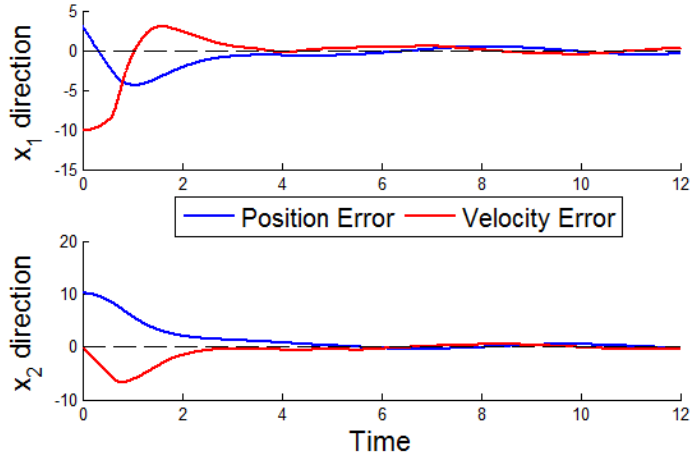

FIGURE 33: Position and Velocity error associated with the evader centrode during case study 6

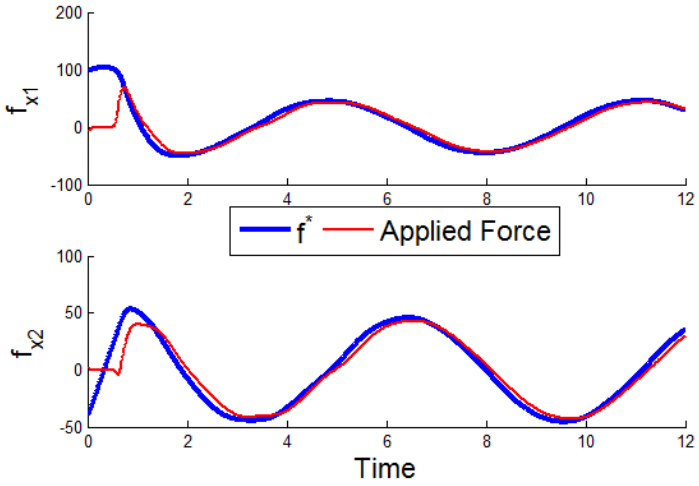

FIGURE 34: Evader control forces

4.5 DRAWBACKS OF THE PADDLE BASED POSITIONING METHOD

The proposed control utilized in the discrete positioning method is effective at herding a group of agents, with a series of PD controllers and carefully selected desired trajectories. The RHSMC is only utilized in the MvN case during phase 2. Although this method is effective, it suffers from several considerable drawbacks.

The first major hurdle related to this method is its claim of quasi-decentralization. The desired trajectories are determined to be the same for all agents, are dependent on initial conditions, and rely on the phase determination (also handled by the centralized portion of the control).

The evader swarm in the presented case has sufficient inter-agent attractions to prevent fragmentation of the group, however there is no concrete method to guarantee that the evader swarm will not be split by the pursuers positioning and repulsions. Note that the radius at which the pursuers are positioned is determined as a multiple of the evader's sensing radius around the swarm centrode and does not take into account the amount of dispersion of the swarm.

Additionally, the control logic to select which swarm should be sent to which desired position is convoluted. As the vector $\mathbf{f}^*$ passes through zero, the position which was defined by $\mathbf{z}_{d2,1} = \mathbf{y} - r \cdot \mathbf{R}(+\Delta\theta) \cdot \frac{\mathbf{f}^*}{\|\mathbf{f}^*\|}$, we see that the unit vector $\frac{\mathbf{f}^*}{\|\mathbf{f}^*\|}$ suddenly switches, and agents positioned at $\mathbf{z}_{d2,1}$ now lie at $\mathbf{z}_{d2,2}$. The

determination of which swarm should be assigned to which position is non-trivial, but not included in this discussion.

In order to remedy all of these shortcomings, we propose a cylindrical coordinate variant of the control which simplifies the operation. The control requires no phase determination, assignment of evaders to one of two points, and can accommodate a splitting swarm.

4.6 ARC BASED RHSMC FOR 2v1 HERDING

For simplicity we again consider a two-pursuer-one-evader (2v1) case. The evader dynamics remains unchanged as in Equation (50) but the inter-agent repulsion term in Equation (1) is composed of a single repulsion. For this scenario a structured pursuer distribution is shown in Figure 35 with the pursuers (blue circles) lying on a circular *frontal arc* (shown as a dashed line) at a uniform distance, r_d, from the evader (red square) and symmetrically located with respect to $\mathbf{f}^*$, at $\theta_d \pm \Delta\theta$ polar angles. Placing pursuers on an arc is the most natural form of herding, as it is inspired from common biological observations.

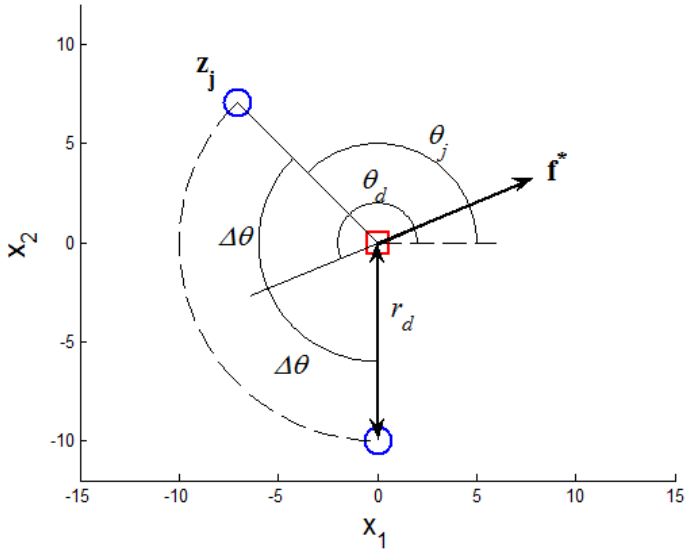

FIGURE 35: Two pursuers placed at the extremes

of a frontal arc centered at the evader

Identically to the developments from Equation (38-40), the magnitude of $\mathbf{f}^*$ plays the determining role. The herding force on the evader becomes

$$\left\|\mathbf{f}^*\right\| = 2\rho \cdot (r_e - r_d) \cdot \cos(\Delta\theta) \tag{62}$$

where $\Delta\theta = \left|\theta_d - \theta_j\right|$ and θ_j is the angle of the vector connecting the evader to pursuer, $\mathbf{z}_j - \mathbf{y}$.

$$r_d = \chi r_{\max} = \chi\left(r_e - \frac{\left\|\mathbf{f}^*\right\|}{2\rho}\right) \qquad 0 < \chi < 1 \tag{63}$$

This choice incites an angle between the pursuers, $2\Delta\theta$, which appropriately applies $\left\|\mathbf{f}^*\right\|$. This is obtained by solving equation (62) for $\Delta\theta$,

$$\Delta\theta = \cos^{-1}\left(\frac{\left\|\mathbf{f}^*\right\|}{2\rho(r_e - r_d)}\right) \tag{64}$$

For logistical preference, in this implementation we bound the smallest arc length to $\frac{\pi}{8} \le \Delta\theta$ to prevent the pursuers from bunching up. This lower bound arises due to the diminishing returns from reduction of $\Delta\theta$, as the force increases. Furthermore it is clear that the upperbound for this arc length is $\Delta\theta < \pi/2$ for a given $\mathbf{f}^*$. Larger angular separation would reverse the direction of $\mathbf{f}^*$. The midpoint of the arc is logically placed in the opposite direction of $\mathbf{f}^*$, meaning the pursuers align behind the evaders in order to herd them,

$$\theta_d = \angle\mathbf{f}^* + \pi \tag{93}$$

Expressions (63, 64, 93) define the arc on which the pursuing agents are placed in order to generate the desired herding force of equation (58). Another critical issue arises when the herding force, $\left\|\mathbf{f}^*\right\|$ becomes small. Similarly to the discrete positioning case, its direction can change rapidly under the influence of the disturbances. One can easily observe that this will incite jumps in the direction of the control action by π. Additionally $\dot{\theta}_d$ and $\ddot{\theta}_d$ terms in equation (46) become indefinitely large. To prevent these occurrences, we propose to switch the compensator off when $\left\|\mathbf{f}^*\right\|$ falls below a response threshold ($\left\|\mathbf{f}^*\right\| < 0.05 f_{ep,\max} = 0.1\rho r_e$).

In the same time one can observe that in equation (31) the $\mathbf{f}_{pp}$ term acts to spread the agents and it is linear in nature. In the angular direction this can be

approximated as a proportional function to $\theta_j - \theta_{eq}$, where θ_{eq} is a stationary equilibrium position relative to other pursuer (in the 2v1 case $\theta_{eq} = 90^\circ$). This brings the angular dynamics of equation (31) to

$$r_j \ddot{\theta}_j = u_{j,\theta} - K\left(\theta_j - \theta_{eq}\right) \tag{94}$$

In order to stabilize the system at the equilibrium positions, we propose a viscous drag term to replace the robust control of equation (46) as

$$u_{j,\theta} = -r_j b_\theta \dot{\theta}_j \tag{95}$$

where b_θ is a selected damping coefficient. The result is a stabilized second order dynamics,

$$r_j \ddot{\theta}_j + r_j b_\theta \dot{\theta}_j + K\left(\theta_j - \theta_{eq}\right) = 0 \tag{96}$$

If and when this $\left\|\mathbf{f}^*\right\|$ threshold condition reverses itself, the original routine, i.e., the control given in equation (46), is resumed.

The objective here is to maintain the pursuers on the defined arc, using local (i.e., decentralized) control schemes. In contrast to the previous method, the pursuers are not individually assigned to follow specific target locations as the operation progresses. They are directed to occupy the dynamically moving frontal arc as a group. The previously developed RHSMC concept [24] is utilized to tackle this mission, considering some of the active force components are unknown to the controller. Here, the region holding controller will direct all agents to the center of the frontal arc using a robust controller against unknown but likely agent-to-agent forces. The controller must be designed to allow these pursuer-to-

pursuer forces to manage their self organized distribution within the target arc. In other words, the robustness features of the controller should be executed preferentially along and orthogonal to the arc. This approach invites the representation of the dynamics in polar coordinates because

a) The desired pursuer positions determined in Section 4.6 and 4.7 are most easily defined by (63, 64, 93) and have polar symmetry with respect to $\mathbf{f}^*$.
b) The below suggested decentralized control scheme can be deployed in polar coordinates without the need for a multiple-phase evaluation.

CASE STUDY 7: 2v1 Arc Based Herding

The first study of the arc based herding control is performed on a 2v1 case. The objective is to bring the evader to a stationary target $\mathbf{y}_d(t) = 0$ and parameters are taken from Table 6. Note that the selection of P_e and D_e creates poles of the evader error dynamics (57) at $p_1 = -2$, $p_2 = -3$. Snapshots of the herding at different instances are shown in Fig 36. The two pursuers are shown as blue circles, the evader as a red square, and the herding target is at the origin.

Evader	Pursuer	Control
$m_e = 1$	$m_p = 1$	$P_e = 6$
$b_e = 1$	$b_p = 1$	$D_e = 4$
$\rho = .5$	$\mu = 15$	$\chi = 0.95$
$r_e = 10$	$r_p = 30$	$\lambda = 10$
		$K_1 = 10$
		$\varepsilon = 10$
		$b = \lambda\pi / 8$
		$b_\theta = 5$

TABLE 5: Case study 7 parameters

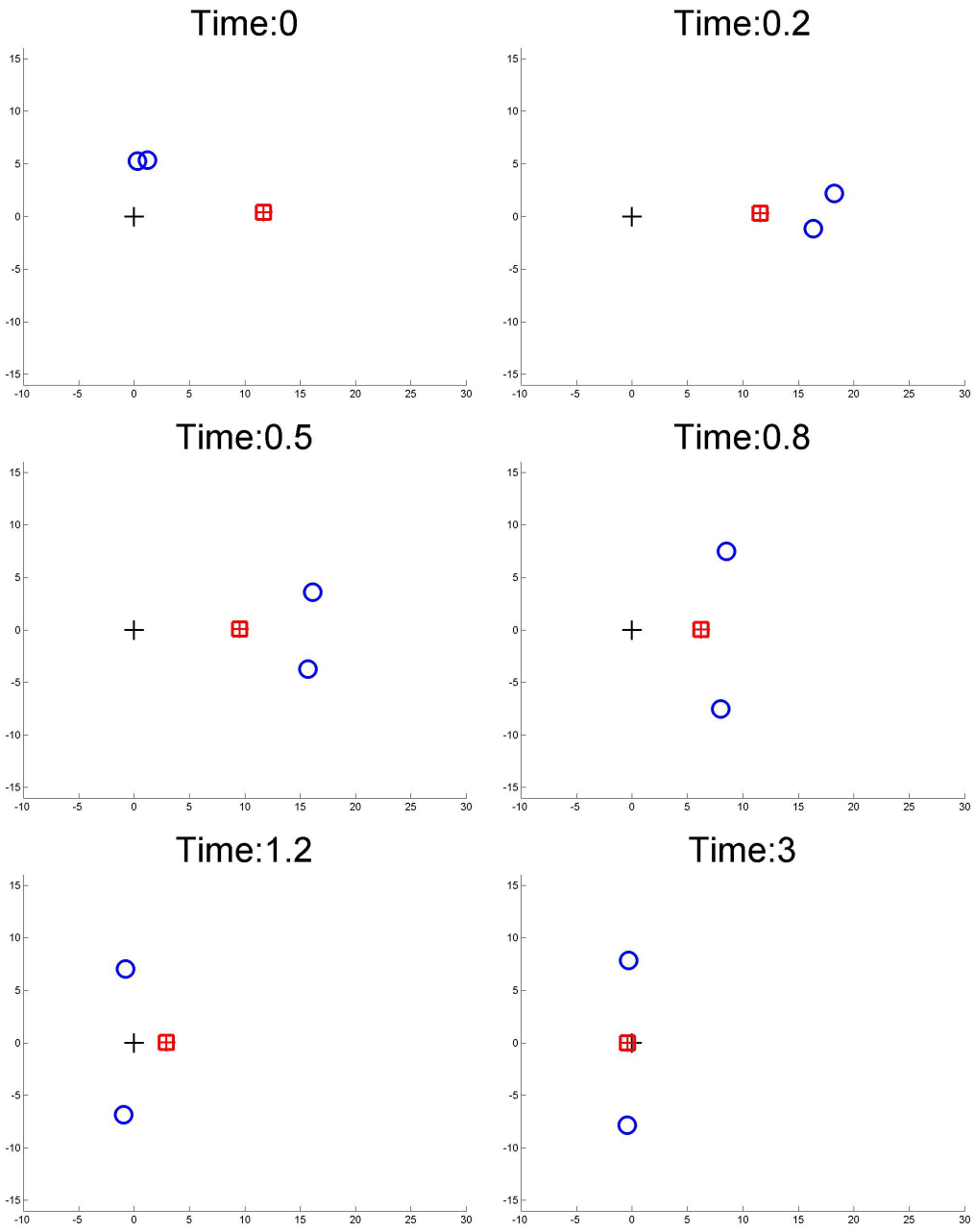

FIGURE 36: Simulation snapshots for case study 6

It is clear that until frame 3 (t=0.5 sec) the pursuers are trying to position themselves behind the evader (herding staging operation). Then the herding takes place in frames 3-6. In fact, the herding force, $\mathbf{f}^*$, is targeted all along, but the

pursuers cannot be positioned properly to execute this force variation with perfection as we see in Fig. 37. Their path *around* the evader is determined by the decay of both the radial and angular dynamics at the same time. This replaces the necessity for a phase 1 operation which was required in the discrete case. We observe in Fig 38, the two components of the evader error vector e_e, resulting from this pursuer positioning effort. The evader error decays in approximately 2 seconds, corresponding to the dominant time constants of the evader error dynamics, as we mentioned over equation (57).

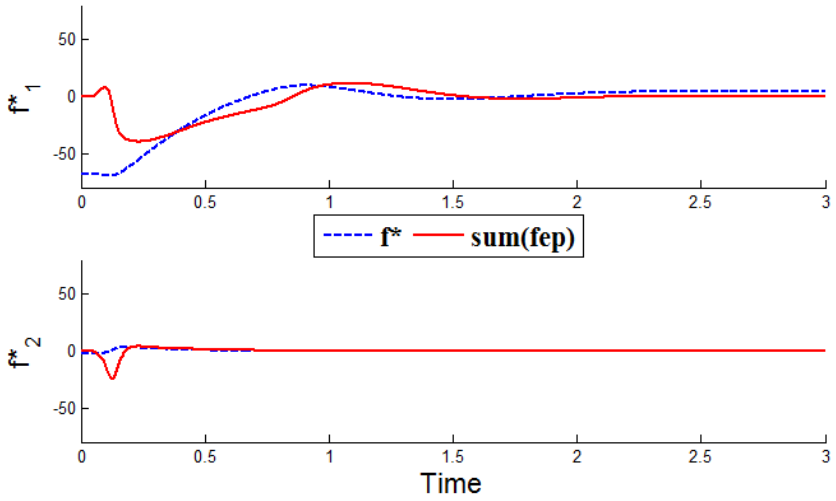

FIGURE 37: Components of the desired herding force (blue dashes) and the executed repulsive forces

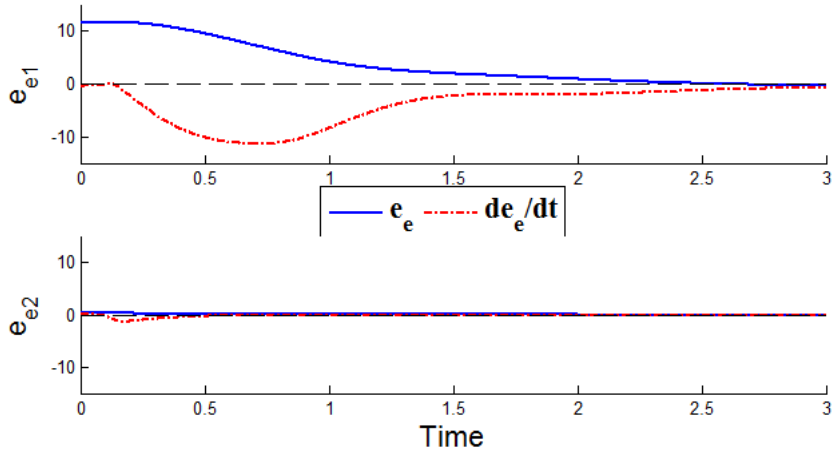

FIGURE 38: Evader error $\mathbf{e_e}$ variation

The total control action taken on each of the pursuers is shown in Fig 39. Notice the aggressive action which takes effect during the pursuers' approach to their herding positions starting from the initial setup. In practice, this control effort will likely saturate and delay the approach of the pursuers towards the evader. Since the repulsion force does not exist outside the evader's sensing range, this feature should not adversely affect the system. The shaded portions of the plot identify the locations where the magnitude of the herding force is below a threshold, where we utilize the viscous damping feature given in (95). We see finite jumps in both control signals as we transition between the two angular controls (28 and 95). This corresponds to the approach phase of the sliding functions, shown in Fig 40. Both sliding functions quickly enter the common boundary layer (shown as red dashed lines). The time varying boundary layer in the angular dimension is related to the desired arc length and changes with the magnitude of the desired herding force $\mathbf{f}^*$. This value is only shown during times where the angular sliding mode control of equation (28) is active, ensuring a

decay to the region and then confinement within the boundary layer. Each agent is pushed to opposite sides of the boundary layer by the repulsion forces.

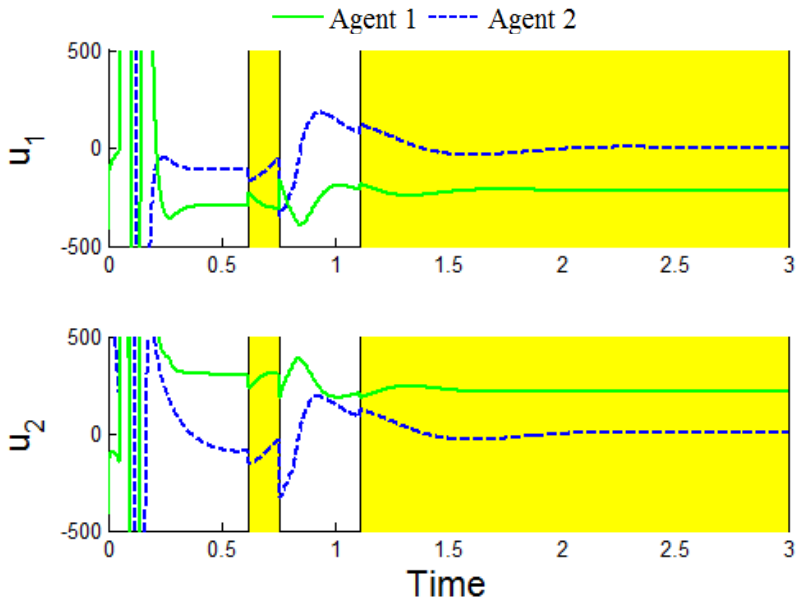

FIGURE 39: Control action on pursuers

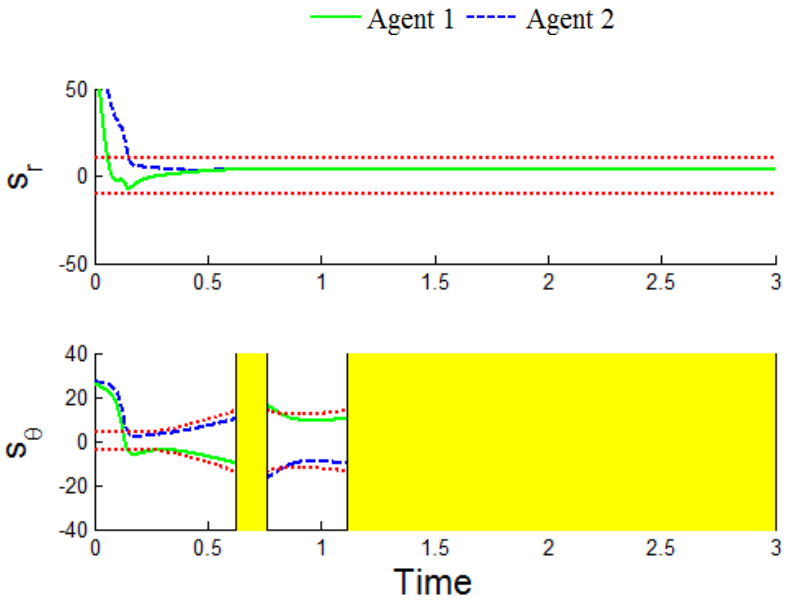

FIGURE 40: Sliding function variations (green and dashed blue) and the boundary layers (short dashed red)

4.7 ARC BASED HERDING IN THE MvN CASE

Introducing additional pursuers to the problem allows us to further increase the robustness of the system, as the herding would be better coordinated using more pursuer agents. As their number increases beyond a certain level, the addition or deletion of a single agent would be insignificant on the performance of the herding.

The 2v1 to MvN expansion requires only small changes to the preceding series of logic, namely the determination of the summation terms in (1) and (30). The feedback control on the evaders is calculated identically to the previous case, using equation (38).

In order to redefine the arc for the case of multiple pursuers, we examine an example distribution as given in Fig. 41.

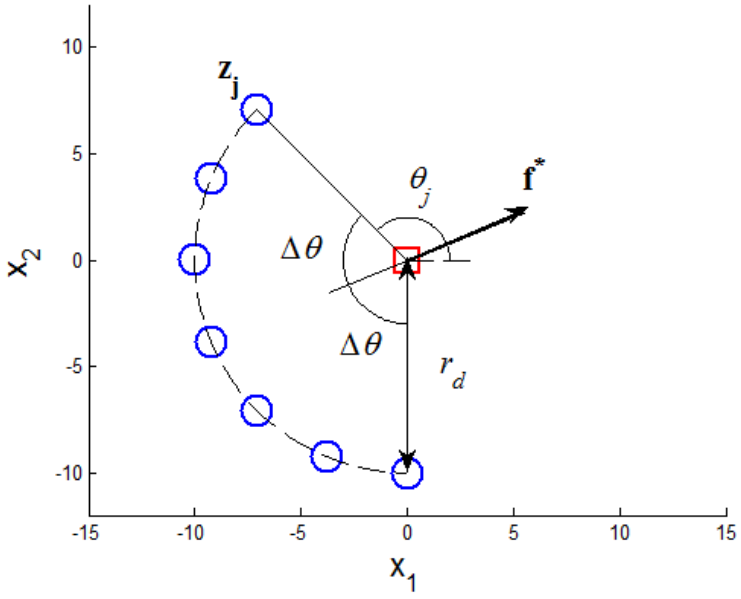

FIGURE 41: 7 pursuers surrounding 1 evader

The desired radius of Eq (63) is slightly modified for additional pursuers by accounting for *M* pursuers in the calculation of $r_{\max}$, and for additional evaders by including the maximum evader swarm radius.

$$r_d = \chi\, r_{\max} = \chi\left(r_e - \frac{\left\|\mathbf{f}^*\right\|}{M\rho}\right) + \max\left(\left\|\mathbf{y}_i - \bar{\mathbf{y}}\right\|\right) \tag{97}$$

Including the evader swarm radius allows us to ensure that the pursuers will never enter the evader swarm perimeter and cannot split the swarm.

The radius prescribed by equation (97) leads to discontinuities in the control action of equation (40) at instants when the agent furthest from the swarm center changes. Although r_d remains continuous at this switch, the velocity does not (or there would be no change in agent), meaning $\dot{r}_d$ and $\ddot{r}_d$ are discontinuous at this instant. In order to prevent this, we pass the calculated desired radius r_d of Eq. (97) through a second order filter with poles $-5K_1$ and -5λ (significantly faster than the pursuer error dynamics poles in the absence of a robustizing term as seen in the case of the discrete controller) and a DC gain of 1. This filtered radius, denoted r_{df}, has two continuous derivatives eliminating the discontinuous control effort in equation (40).

The determination of arc length is found by reexamining the repulsions in equation (58) for the multiple pursuer case

$$\left\|\sum_{j=1}^{M}\mathbf{f}_{ep,\bar{\mathbf{y}},j}\right\| = \left\|\mathbf{f}^*\right\| = \sum_{i=1}^{M}\rho\cdot\left(r_e - r_{df}\right)\cdot\cos\left(\theta_d - \theta_j\right) \tag{98}$$

By solving (98) for the arc length, $\Delta\theta$, using the filtered radius, the magnitude of $\mathbf{f}^*$ is still properly applied and there is no change in the effectiveness of the

positioning scheme. Ideally we expect to have the pursuer agents distributed with a uniform separation distance of $\frac{2\Delta\theta}{M-1}$ along the frontal arc of $2\Delta\theta$. They will, in ensemble, execute the herding force $\mathbf{f}^*$ and the following should hold:

$$\left\|\sum_{j=1}^{M}\mathbf{f}_{ep,\bar{\mathbf{y}},j}\right\| = \left\|\mathbf{f}^*\right\| = \sum_{i=1}^{M}\rho\cdot\left(r_e - r_{df}\right)\cdot\cos\left((i-1)\frac{2\Delta\theta}{M-1} - \Delta\theta\right) \qquad (99)$$

By solving equation (99) for $\Delta\theta$, we can properly select the boundary layer size in equation (46) and (47), which restricts our agents to the correctly sized arc. In order to solve equation (99) for $\Delta\theta$, we expand the $\cos(nq)$ terms into a polynomial of $\cos(q)$ of degree *n* a priori. At each simulation step we then solve the polynomial for $\cos(q)$ using MATLAB root finding routines and subsequently solve for *q*.

The desired center of the arc should remain opposite to the herding force, as indicated by equation (58). The control of the pursuers is still performed according to Section 3.3 with equations (28), (40) and (46). In the case where $\left\|\mathbf{f}^*\right\| \approx 0$, we again utilize our damping treatment from equation (95). Noting that there continues to exist an equilibrium configuration distributed around the entire circle ($2\Delta\theta = 2\pi$) we replace the sliding mode controller with a viscous drag term. The only change required is to modify the evaluation of the most pessimistic scenario using

$$f_{pp,\max} = (M-1)r_p\mu \geq \left\|\sum_{\substack{k=1\\k\neq j}}^{M}\mathbf{f}_{pp,j,k}\right\| \qquad (100)$$

These changes allow us to claim robust adherence to the modified frontal arc region by the *M* pursuers.

CASE STUDY 8: MvN Arc Based Herding

We next consider a case of 10v10, and apply the positioning logic in Section 4.7. In this case we deploy the parameters from Table 6. The summation in equation (99) is written

$$\left\|\mathbf{f}^*\right\| = \rho\cdot\left(r_e - r_{df}\right)\cdot 2\left[\cos\left(\tfrac{1}{9}\Delta\theta\right)+\cos\left(\tfrac{3}{9}\Delta\theta\right)+\cos\left(\tfrac{5}{9}\Delta\theta\right)+\cos\left(\tfrac{7}{9}\Delta\theta\right)+\cos\left(\Delta\theta\right)\right]$$

Expanding the cosine terms, one can find a polynomial in $\cos\left(\tfrac{1}{9}\Delta\theta\right)$ as

$$\frac{\left\|\mathbf{f}^*\right\|}{\rho\cdot\left(r_e - r_{df}\right)} = 512\cos\left(\tfrac{1}{9}\Delta\theta\right)^9 - 1024\cos\left(\tfrac{1}{9}\Delta\theta\right)^7 + 672\cos\left(\tfrac{1}{9}\Delta\theta\right)^5 - 160\cos\left(\tfrac{1}{9}\Delta\theta\right)^3 + 10\cos\left(\tfrac{1}{9}\Delta\theta\right)$$

The real valued solutions that are in [-1,+1] are considered only. Additionally, $\Delta\theta$ must be bounded as $0 \le \Delta\theta \le \tfrac{9}{10}\pi$. It can be shown via root locus plots that this equation only has one root which satisfies this condition. Intuitively, this makes geometric sense as well that there should only be one solution for $\Delta\theta$ in the herding force magnitude equation. This further leads to the value of $\cos\left(\tfrac{1}{9}\Delta\theta\right)$ to be bounded as $\cos\left(\tfrac{\pi}{10}\right) \le \cos\left(\tfrac{1}{9}\Delta\theta\right) \le 1$. The corresponding $\Delta\theta$ is determined within the algorithm at each instant, as $\left\|\mathbf{f}^*\right\|$ and r_{df} vary in time.

For this case study, we utilize a desired herding trajectory $\mathbf{y}_d(t) = \left[15\cdot t,\ \ 30\sin(t)\right]^T$ instead of a fixed target location. Figure 42 shows that trajectory and the pursuer distribution at several snapshots. The black dashed line

indicates the desired trajectory. Snapshots of the agents are shown at 3 second intervals and the path of the evader is shown with the red line. Figure 43 shows a history of the evader's position error with respect to the trajectory and its derivative. The settling time of approximately 2.5 seconds is due to both the dominant time constant and the approach phase of the pursuers.

Evader	Pursuer	Control
$m_e = 1$	$m_p = 1$	$P_e = 6$
$b_e = 1$	$b_p = 1$	$D_e = 4$
$\rho = 1$	$\mu = 5$	$\chi = 0.50$
$r_e = 20$	$r_p = 20$	$\lambda = 10$
$\alpha = 20$		$K_1 = 10$
$\beta = 20/3$		$\varepsilon = 10$
$\gamma = 1/3$		$b = \lambda\pi/8$
		$b_\theta = 5$

TABLE 6: Case study 8 parameters

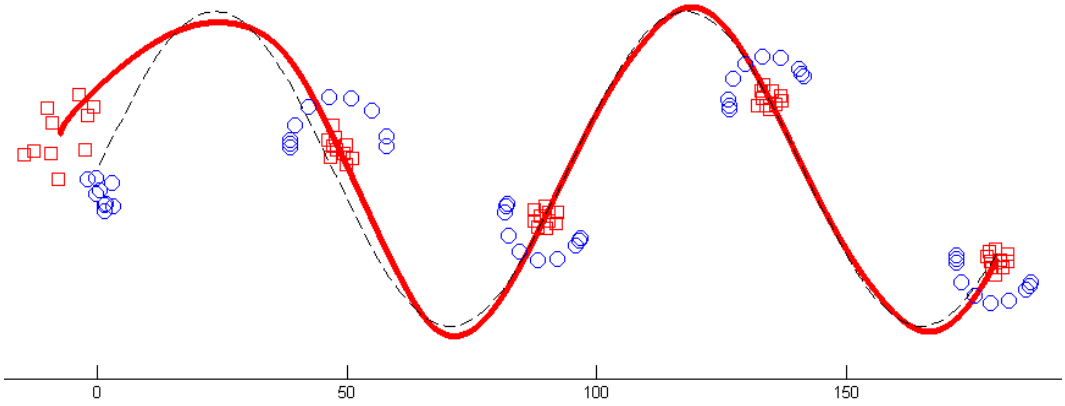

FIGURE 42: 10 Pursuer- 10 evader positions during herding.

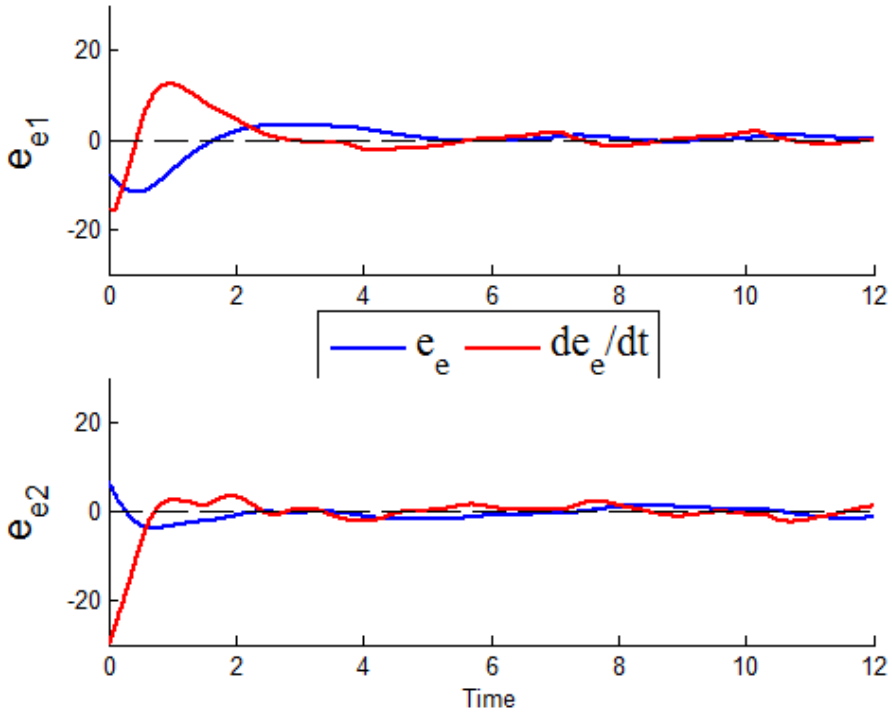

FIGURE 43: Evader error

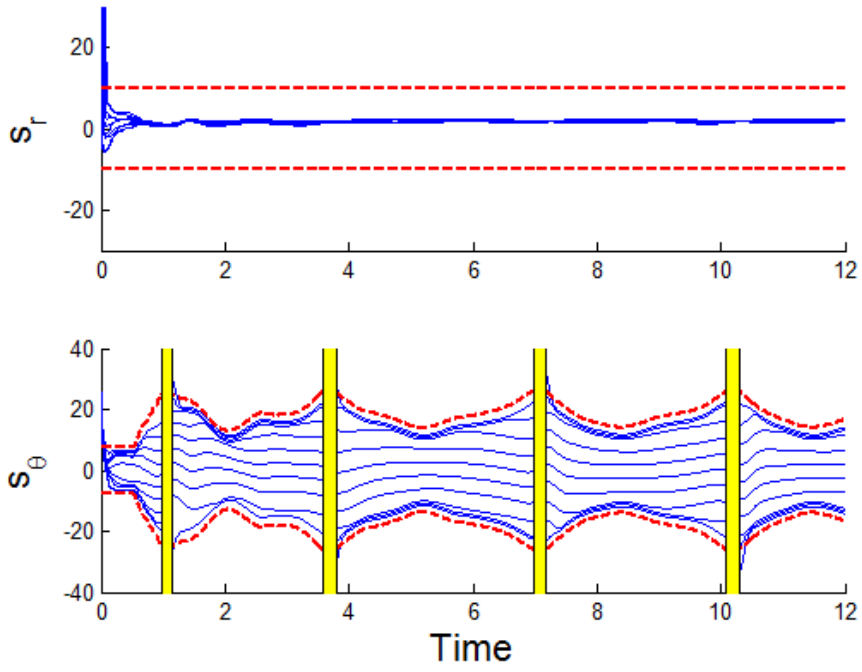

FIGURE 44: Pursuer sliding functions

We can see in Fig. 44 that the sliding functions of all agents are brought within the boundary layer almost instantaneously, and that the distributions of sliding functions in the angular direction are well spaced, while being robustly contained. We see moments where the force dips below the threshold of which requires the use of equation 95. As a result, for a brief period, the proper herding force is not applied and we see in Figure 42 that the agents slightly overshoot their desired trajectory.

5. CONCLUSIONS

In this thesis we present a decentralized, scalable, sliding mode controller capable of driving individual agents of a swarm into desired regions while maintaining a roughly uniform distribution. The controller contains the strengths of traditional sliding mode control methodology for disturbance rejection and the mitigation of modeling uncertainty. The primary difference is the use of a novel boundary layer concept for multi-agent 'swarms'. When all agents share the identical goal and utilize the same control, we can claim robust adherence to a specific geometric region. The inter-agent repulsions between the agents work to create a distribution about the common desired position. For the case of circular and elliptical targets, a way of estimating these upperbounds is also presented.

The control itself is decentralized in that each agent only requires information about the region's center, its maximum deviation in each direction, and the maximum repulsion and uncertainty force it must overcome. The agents become aware of other agents in their neighborhood. In this implementation, this also corresponds to a claim of connectedness of the topology. When the inter-agent repulsions are the dominant uncertainty, agents are driven to the regions' center robustly until they come into the interaction radius of other agents, thus connecting the swarm.

Although the assumed distributions for circular and elliptical targets were all calculated in a 2-D space, the controller logic is scalable for higher dimensions.

Additionally, we have leveraged the RHSMC to enable groups of pursuers to herd a group of evader along a desired trajectory using only the known agent dynamics. A centralized evaluation of the evader's states calculates a desired feedback force for the pursuers to apply, and positions at which this force is created are calculated. These desired positions are then passed to the individual pursuers which generate their own control action and accommodate local interactions with other pursuers.

The first implementation of this force relied on a three phase pursuer action, conceived initially as a PD style control. During the intermediate act of herding, in the presence of multiple pursuers, the PD controller is enhanced by the robustizing properties of SMC to further restrict pursuer positions, ensuring an even force application.

This implementation suffered several problems related to the claims of decentralization, in that the control phases were declared by a centralized control, tying all agents together. Additionally the agents were split into two known groups a priori.

A new method of pursuer control via RHSMC improved upon this by utilizing cylindrical coordinates. The coordinate change allowed the implementation of a single arc-shaped region defined by an orientation, arc length, and radius. The sliding mode control elements acted in the radial and tangential directions to reduce the error. In the radial direction, error was limited to a small manageable distance, while in the tangential direction the error was left

large corresponding to the arc length and the agents were allowed to distribute themselves evenly within.

REFERENCES

[1] Murray, R.M., 2007, “Recent Research in cooperative control of multi-vehicle systems” *Journal of Dynamic Systems, Measurement and Control*. Vol. 129, 571-583

[2] Warburton, K., Lazarus, J., “Tendency-distance models of cohesion in animal groups”, *Journal of Theoretical Biology*, Vol 150, 473-488

[3] Camazine, S., Deneubourg, J., and N.R. Franks, 2001, Self Organization in Biological Systems. Princeton University Press

[4] Reynolds, C.W., 1987, “Flocks, herds and schools: A distributed behavioral model,” *Computer Graphics*, Vol. 21

[5] Gazi, V., Passino, K.M., 2003, “Stability Analysis of Swarms”, IEEE Transaction on Automatic Control, Vol 48

[6] Gazi, V., Passino K. M., 2004, “A Class of Attractions / Repulsion Functions for Stable Swarm Aggregations”, *International Journal of Control,* Vol. 77, 1567-1579

[7] Olfati-Saber, R., 2006, “Flocking for Multi-Agent Dynamic Systems: Algorithms and Theory”, *IEEE Transactions on Automatic Control*, Vol 51, 401-420

[8] Housheng Su, Xiaofan Wang, Zongli Lin, 2009, "Flocking of Multi-Agents With a Virtual Leader", *IEEE Transactions on Automatic Control*, Vol. 54

[9] Tanner, H.G., Jadbabaie, A., Pappas, G.J., 2007, "Flocking in Fixed and Switching Networks", *IEEE Transactions on Automatic Control*, Vol. 52

[10] Zavlanos, M.M., Tanner, H.G., 2009, "Hybrid Control for Connectivity Preserving Flocking", *IEEE Transactions on Automatic Control*, Vol 53

[11] Yao, J., Ordonez, R., Gazi, V., 2007, "Swarm tracking using artificial potentials and sliding mode control", *Journal of Dynamic Systems, Measurement and Control,* Vol. 129, 749-754

[12] Cortes, J.,Martinez, S., Karatas, T., Bullo, F., 2004, "Coverage control for mobile sensing networks", *IEEE Transactions on Robotics and Automation* Vol. 20, 243-255.

[13] Laventall, K., Cortes, J., 2009, "Coverage control by multi-robot networks with limited-range anisotropic sensory", *International Journal of Control*, Vol. 82, 1113-1121

[14] Bullo, F., Cortes, J., Martinez, S., 2009, Distributed Control of Robotic Networks, Princeton University Press

[15] Cheah, C.C., Hou, S.P., Slotine, J.J., 2009, "Region-based shape control for a swarm of robots", *Automatica*, Vol. 45, 2406-2411

[16] McCullough, P., Bacon, M., Olgac, N., Sierra, D.A., Cepeda-Gomez, R., 2010, "A Lyapunov Treatment of Swarm Coordination Under Conflict", *Journal of Vibrations and Controls*, Available Online

[17] Utkin, V.I., 1977, "Variable Structure Systems with Sliding Modes", IEEE Transactions on Automatic Control, Vol AC-22, pp 212-222

[18] Slotine, J.J., 1984, “Sliding controller design for non-linear systems”, *International Journal of Control*, Vol 40, 421-434

[19] Elmali, H., Olgac, N., 1992, “Sliding mode control with perturbation estimation (SMCPE): a new approach”, *International Journal of Control* Vol 56, 923-941

[20] LaSalle, J., 1960, “Some Extensions of Liapunov’s Second Method”, *IRE Transactions on Circuit Theory,* Vol 7, 520-527

[21] Kachroo, P., Shedied, S.A., Bay, J.S., Vanlandingham, H., 2001, “Dynamic Programming Solution for a Class of Pursuit Evasion Problems: The Herding Problem”, *IEEE Transactions on Systems, Man, and Cybernetics*, Vol. 31, 35-41

[22] Lien, J., Bayazit, O.B., Sowell, R.T., Rodriguez, S., Amato, N.M., 2004, “Shepherding Behaviors”, Proceedings of the 2004 IEEE International Conference on Robotics and Automation, Vol 4, 4159-4164

[23] Lien, J., Rodriguez, S., Malric, J., Amato, N.M, 2005, “Shepherding Behaviors with Multiple Shepherds”, Proceedings of the 2005 IEEE Conference on Robotics and Automation, 3402-3407

[24] Bacon, M., Olgac, N., 2010, “Robust region-tracking for multi-agent systems using sliding mode control”, ASME 2010 Dynamic Systems and Controls Conference

[25] Jin, D., Gao, L, 2008, “Stability Analysis of a Double Integrator Swarm Model Related to Position and Velocity”, *Transactions of the Institute of Measurement and Control*, Vol. 30, 275-293